Article

Not peer-reviewed version

# Nanoencapsulated *Dunaliella tertiolecta* Extract and β-Carotene in Liposomal Carriers: Antioxidant and Erythroprotective Po-tential through Sustained Release Systems

Jonathan García-Morales , Ricardo Iván González-Vega * , Diana Fimbres-Olivarría , Ariadna Thalía Bernal-Mercado , Santiago Pedro Auobourg-Martínez , Karla Alejandra López-Gastélum , Silvia Elena Burruel-Ibarra , María Irene Silvas-García , Andrea Grijalva-Molina , José de Jesús Ornelas-Paz , Carmen Lizette Del-Toro-Sánchez *

Posted Date: 7 August 2025

doi: 10.20944/preprints202508.0483.v1

Keywords: *Dunaliella tertiolecta*; β-carotene; nanoliposomes; nanoencapsulation; antioxidant activity; erythroprotective effect; sustained release; oxidative stress

*Article*

# Nanoencapsulated *Dunaliella tertiolecta* Extract and β-Carotene in Liposomal Carriers: Antioxidant and Erythroprotective Potential through Sustained Release Systems

**Jonathan García-Morales [1], Ricardo Iván González-Vega [2,*], Diana Fimbres-Olivarría [3], Ariadna Thalía Bernal-Mercado [1], Santiago Pedro Auobourg-Martínez [4], Karla Alejandra López-Gastelum [1], Silvia Elena Burruel-Ibarra [5], María Irene Silvas-García [1], Andrea Grijalva-Molina [1] José de Jesús Ornelas-Paz [6] and Carmen Lizette Del-Toro-Sánchez [1,*]**

[1] Department of Research and Postgraduate in Food, University of Sonora, Blvd Luis Encinas y Rosales S/N, Col. Centro, Hermosillo 83000, SO, Mexico

[2] Department of Health Sciences, University Center of the Valleys (CUVALLE), University of Guadalajara, Carr. a Guadalajara Km. 45.5, Ameca 46600, JA, Mexico

[3] Departamento de Investigaciones Científicas y Tecnológicas. Universidad de Sonora, Blvd Luis Donaldo Colosio W/N, Hermosillo, Sonora, México. Z.C. 83000

[4] Departamento de Tecnología en Alimentos. Instituto de Investigaciones Marinas (CSIC). Av. Eduardo Cabello No. 6, Vigo, Penevedra, España. Z.C. 36208

[5] Departamento de Investigación en Polímero y Materiales, Universidad de Sonora, Blvd. Luis Encinas y Rosales S/N, Col. Centro, Hermosillo 83000, Sonora, Mexico

[6] Centro de Investigación en Alimentación y Desarrollo A.C.-Unidad Cuauhtémoc, Av. Río Conchos S/N, Parque Industrial, Ciudad Cuauhtémoc 31570, Chihuahua, Mexico

* Correspondence: ricardo.gonzalez@academicos.udg.mx (R.I.G.-V.); carmen.deltoro@unison.mx (C.L.D.-T.-S.)

**Abstract**

The nanoencapsulation of bioactive compounds such as β-carotene and microalgal extracts has emerged as an effective strategy to enhance their stability, bioavailability, and biological efficacy. *Dunaliella tertiolecta*, a microalga rich in carotenoids and chlorophylls, presents notable antioxidant and erythroprotective properties; however, its bioactive potential is limited by low bioaccessibility and degradation during processing and digestion. This study aimed to develop and evaluate nanoliposomes loaded with *D. tertiolecta* extract and β-carotene as sustained-release systems to improve antioxidant performance and erythroprotective effects. The methodology involved optimizing microalgal cultivation under nitrogen and salinity stress to enhance pigment accumulation, followed by extraction, nanoencapsulation via the particle dispersion method, and physicochemical characterization of the nanoliposomes. Antioxidant capacity and release kinetics were assessed through ABTS and FRAP assays, while erythroprotective activity was evaluated by monitoring oxidative hemolysis in human erythrocytes. The release kinetics revealed an anomalous transport mechanism for both systems, with β-carotene showing faster and more efficient release due to its greater lipophilic compatibility with the nanoliposomal matrix. The nanoliposomal systems demonstrated nanoscale size, high encapsulation efficiency, sustained antioxidant release, and effective erythrocyte protection, with the extract-loaded formulation exhibiting synergistic effects superior to isolated β-carotene. These findings support the potential application of this nanotechnology-based delivery system in functional foods, nutraceuticals, and biomedical formulations aimed at preventing oxidative stress-related cellular damage.

**Keywords:** *Dunaliella tertiolecta*; β-carotene; nanoliposomes; nanoencapsulation; antioxidant activity; erythroprotective effect; sustained release; oxidative stress

 doi:10.20944/preprints202508.0483.v1



## 1. Introduction

Oxidative stress, characterized by an imbalance between the production of reactive oxygen species (ROS) and the antioxidant defense mechanisms of the organism, plays a central role in the pathogenesis of various chronic and degenerative diseases, including cardiovascular disorders, diabetes, anemia, and cancer [1,2]. At the molecular level, ROS such as superoxide anion ($O_2^{\bullet -}$), hydroxyl radical (•OH), and hydrogen peroxide ($H_2O_2$) induce lipid peroxidation, protein oxidation, and DNA damage, compromising cellular integrity and function [3–6]. Antioxidant molecules counteract these deleterious effects through mechanisms including hydrogen atom transfer (HAT), where hydrogen atoms are donated to neutralize free radicals, and single electron transfer (SET), where electrons are donated to stabilize reactive species [7–9]. Carotenoids such as β-carotene and chlorophyll derivatives exert potent antioxidant effects by quenching singlet oxygen ($^1O_2$) and scavenging peroxyl radicals, contributing to membrane stabilization and protection of cellular structures [10,11]. However, the efficacy of these compounds is limited by their hydrophobic nature, low aqueous solubility, and susceptibility to oxidative degradation during processing and gastrointestinal digestion.

In recent years, nanoencapsulation technologies have emerged as powerful tools to improve the stability, bioavailability, and functionality of bioactive compounds. Among these, nanoliposomes—nanoscale vesicles composed of phospholipid bilayers—offer significant advantages as delivery systems due to their amphiphilic architecture, which enables the encapsulation of both hydrophobic and hydrophilic molecules [12,13]. This structural arrangement protects sensitive compounds from environmental factors such as light, oxygen, and pH fluctuations, while promoting controlled and sustained release [14–16]. Prior studies have successfully employed nanoliposomal encapsulation for various carotenoids, including fucoxanthin and astaxanthin, demonstrating improvements in their antioxidant activity, bioaccessibility, and cellular uptake. Furthermore, microalgal extracts from species such as *Haematococcus pluvialis*, *Chlorella vulgaris*, and *Spirulina platensis* have been incorporated into nanocarriers, enhancing their functional performance [17–19]. However, despite these advances, the encapsulation of *Dunaliella tertiolecta* extracts, rich in a diverse pool of carotenoids and chlorophylls, remains poorly explored, particularly in systems designed for sustained release and erythroprotective applications.

To date, no studies have comprehensively addressed the nanoencapsulation of *D. tertiolecta* extract and β-carotene in nanoliposomal carriers for the dual purpose of antioxidant delivery and erythrocyte membrane protection against oxidative damage. The nanoencapsulation of carotenoids into nanoliposomes enhances their chemical stability, protects them from oxidative degradation, and improves their solubility and bioavailability in biological systems. This encapsulation strategy enables the sustained and controlled release of the bioactive compounds, allowing a gradual interaction with reactive oxygen species and prolonging their antioxidant action over time. By maintaining effective concentrations of carotenoids at the target site, nanoliposomes optimize the scavenging of free radicals and support continuous membrane protection [20–22]. This prolonged release profile is crucial to maximize the therapeutic potential of carotenoids in preventing oxidative stress-related cellular damage [23]. This represents a significant gap in the current literature, as previous research has focused primarily on isolated carotenoids or other microalgal species without integrating synergistic pigment mixtures in encapsulation strategies [18,19]. The innovative contribution of this research lies in the design, development, and evaluation of nanoliposomes loaded with both β-carotene and *D. tertiolecta* extract, focusing on their physicochemical characterization, sustained antioxidant release behavior, and erythroprotective potential under oxidative stress conditions. This approach provides a novel platform for maximizing the bioactivity of complex natural extracts through nanotechnology, addressing critical challenges in the stability and bio efficacy of carotenoids and chlorophylls.

Therefore, the main objective of this study was to develop and characterize nanoliposomes encapsulating *Dunaliella tertiolecta* extract and β-carotene, evaluating their antioxidant capacity and erythroprotective effects through a sustained release system. This work aims to contribute to the

 doi:10.20944/preprints202508.0483.v1



advancement of functional delivery technologies with potential applications in the food, nutraceutical, and biomedical industries. In perspective, these nanoliposomal formulations may be incorporated into functional foods or health-promoting supplements designed to prevent oxidative stress-related disorders and improve cellular health.

## 2. Results and Discussions

### *2.1. Growth Kinetics of Dunaliella tertiolecta*

The growth kinetics of microalgae provide valuable insights into their cellular proliferation dynamics and metabolic responses under varying environmental conditions. In this study, the growth behavior of Dunaliella tertiolecta was systematically evaluated over a 21-day period under different nitrogen concentrations (0.88, 0.44, and 0.22 mol·L$^{-1}$ of $NaNO_3$) and salinity levels (25, 35, and 45 PSU). Cell density, expressed as $Log_2$ cell/mL, was monitored daily to characterize the distinct growth phases, including lag, exponential, and stationary stages. This approach allowed for the assessment of how nutrient availability and osmotic stress influence the growth performance of D. tertiolecta, providing a basis for understanding the optimal conditions required to maximize biomass accumulation and potential pigment production. The following sections describe and discuss in detail the growth kinetics observed under each experimental condition.

Figure 1 shows the growth kinetics of Dunaliella tertiolecta, expressed as $Log_2$ cell/mL, cultivated at 25 PSU under three different nitrogen concentrations: 0.88 mol·L$^{-1}$, 0.44 mol·L$^{-1}$, and 0.22 mol·L$^{-1}$ of $NaNO_3$. The cultures were monitored over a 21-day period to evaluate the influence of nitrogen availability on cell proliferation. The results demonstrate a clear dependency of microalgal growth on nitrogen concentration. The highest cell density was consistently observed in cultures supplemented with 0.88 mol·L$^{-1}$ $NaNO_3$, indicating that nitrogen sufficiency strongly promotes cellular proliferation and biomass accumulation in D. tertiolecta. Cultures at this concentration exhibited a rapid exponential growth phase within the first 5 to 7 days, reaching a peak of approximately 21 $Log_2$ cell/mL, followed by a stationary phase that remained stable until the end of the experiment. In contrast, the intermediate nitrogen concentration (0.44 mol·L$^{-1}$) also supported robust growth, though the maximum cell density achieved was slightly lower than that observed at 0.88 mol·L$^{-1}$. The growth curve displayed a similar exponential trend but plateaued at around 20 $Log_2$ cell/mL. This suggests that while 0.44 mol·L$^{-1}$ $NaNO_3$ is sufficient to sustain cell division and biomass production, it may not fully meet the nitrogen demands required for maximal proliferation under the given culture conditions.

 doi:10.20944/preprints202508.0483.v1



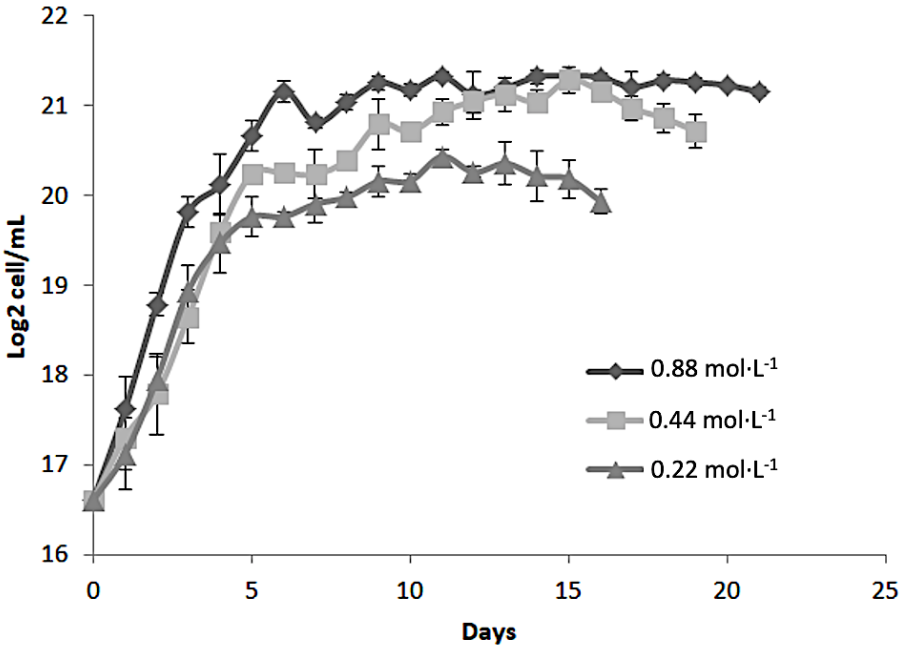


**Figure 1.** Growth kinetics (log2 cell/mL) of the microalgae Dunaliella tertiolecta at 25 PSU in different nitrogen concentrations (0.88 mol·L-1, 0.44 mol·L-1and 0.22 mol·L-1 of NaNO3).

The lowest nitrogen concentration tested (0.22 mol·L$^{-1}$ $NaNO_3$) led to the poorest growth performance. Cultures at this level showed a shortened exponential phase, reaching a maximum of ~19 $Log_2$ cell/mL, with an earlier onset of the stationary phase compared to other treatments. This early arrest is attributed to nitrogen limitation, which restricts protein synthesis, nucleic acid metabolism, and chlorophyll production, ultimately inhibiting cell division and biomass accumulation [24]. These results align with previous studies emphasizing nitrogen's essential role in microalgal growth and metabolism [24,25]. As a key macronutrient, nitrogen is involved in the synthesis of amino acids, nucleotides, and pigments like chlorophylls and carotenoids, which are vital for photosynthesis and cellular function [26]. The observed growth differences highlight the need to optimize nitrogen levels to boost microalgal productivity, especially when aiming to maximize biomass or secondary metabolite production, such as antioxidant pigments [24–27].

Overall, the growth behavior of D. tertiolecta under varying nitrogen regimes suggests that 0.88 mol·L$^{-1}$ $NaNO_3$ provides the most favorable conditions for cell proliferation and biomass accumulation. However, suboptimal nitrogen levels not only limit growth but may also trigger metabolic shifts toward the accumulation of stress-related secondary metabolites, such as carotenoids, which could be beneficial depending on the intended application [28].

Figure 2 illustrates the growth kinetics of Dunaliella tertiolecta, represented as $Log_2$ cell/mL, cultivated at 35 PSU salinity under three nitrogen regimes: 0.88 mol·L$^{-1}$, 0.44 mol·L$^{-1}$, and 0.22 mol·L$^{-1}$ of $NaNO_3$. The cultures were monitored for 21 days to assess the impact of nitrogen concentration on the microalgal proliferation at elevated salinity conditions. The results indicate that nitrogen availability significantly influences the growth performance of D. tertiolecta at 35 PSU. The culture supplemented with the highest nitrogen concentration (0.88 mol·L$^{-1}$ $NaNO_3$) achieved the greatest cell density, reaching approximately 21 $Log_2$ cell/mL during the stationary phase [29]. Similar to the behavior observed at 25 PSU, this treatment exhibited a rapid exponential growth phase within the initial 5 to 7 days, followed by stabilization of cell density, suggesting that sufficient nitrogen supply supports sustained biomass accumulation even under higher salinity stress [30].

 doi:10.20944/preprints202508.0483.v1



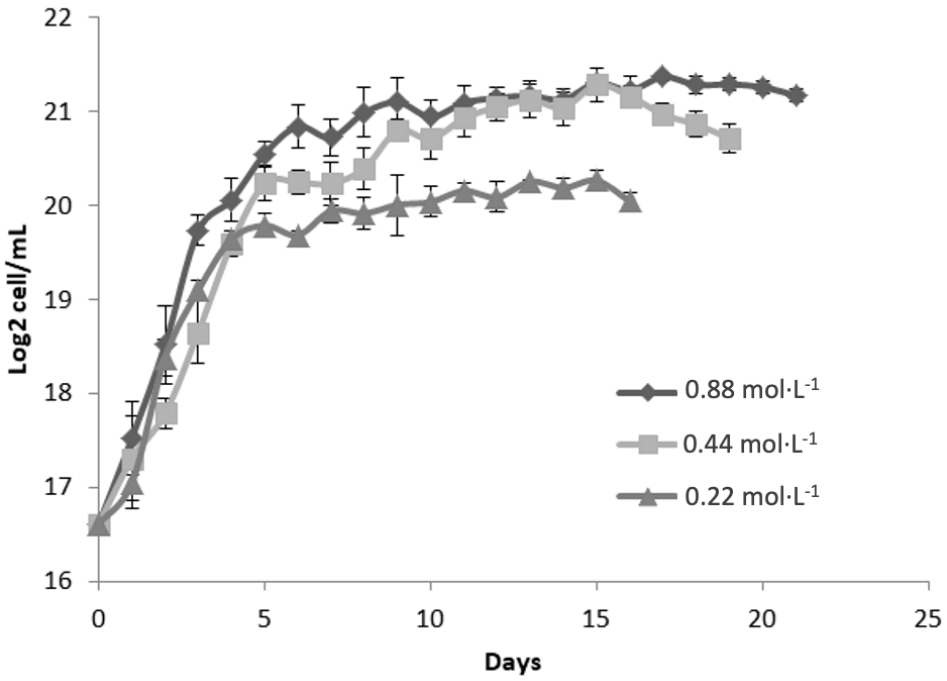


**Figure 2.** Growth kinetics (log2 cell/mL) of the microalgae Dunaliella tertiolecta at 35 PSU in different nitrogen concentrations (0.88 mol·L-1, 0.44 mol·L-1and 0.22 mol·L-1of NaNO3).

Cultures grown with 0.44 mol·L$^{-1}$ $NaNO_3$ showed similar growth kinetics during the exponential phase, though the maximum cell concentration was slightly lower than that of the 0.88 mol·L$^{-1}$ treatment. This suggests that moderate nitrogen levels support cell proliferation but may not meet the full nitrogen demands for optimal biomass under saline conditions. In contrast, cultures with 0.22 mol·L$^{-1}$ $NaNO_3$ exhibited significantly lower growth rates and reached the lowest cell density (~19 $Log_2$ cell/mL), with an earlier stationary phase. This reflects nitrogen limitation, which restricts key biosynthetic processes such as protein, nucleic acid, and pigment synthesis [31].

Comparing growth at 35 PSU with 25 PSU (Figure 1), a slight decline in maximum cell densities was observed across all nitrogen levels, suggesting that increased salinity imposes additional osmotic stress, affecting cell homeostasis and metabolism. Nevertheless, nitrogen supplementation at 0.88 mol·L$^{-1}$ appears to mitigate these effects, supporting sustained growth. These patterns highlight the essential role of nitrogen in maintaining cell function and biomass under saline stress. As a key nutrient in the biosynthesis of essential components, nitrogen limitation disrupts both cell proliferation and metabolic pathways tied to stress responses and secondary metabolite production. Elevated salinity further increases nitrogen demand due to the energy required for osmoregulation and compatible solute synthesis [29–32].

Figure 3 presents the growth kinetics of Dunaliella tertiolecta, expressed as $Log_2$ cell/mL, cultivated at a salinity of 45 PSU with three nitrogen concentrations: 0.88 mol·L$^{-1}$, 0.44 mol·L$^{-1}$, and 0.22 mol·L$^{-1}$ of $NaNO_3$. The culture performance was evaluated over 21 days to determine the effect of nitrogen availability on microalgal proliferation under high-salinity stress conditions. The results demonstrate that nitrogen concentration exerts a significant influence on cell growth, even under elevated salinity. The highest nitrogen concentration (0.88 mol·L$^{-1}$ $NaNO_3$) consistently supported the greatest biomass accumulation, achieving a maximum of approximately 21 $Log_2$ cell/mL. This treatment exhibited a well-defined exponential growth phase during the first 5 to 7 days, followed by the onset of the stationary phase, where cell densities remained stable until the end of the experimental period.

 doi:10.20944/preprints202508.0483.v1



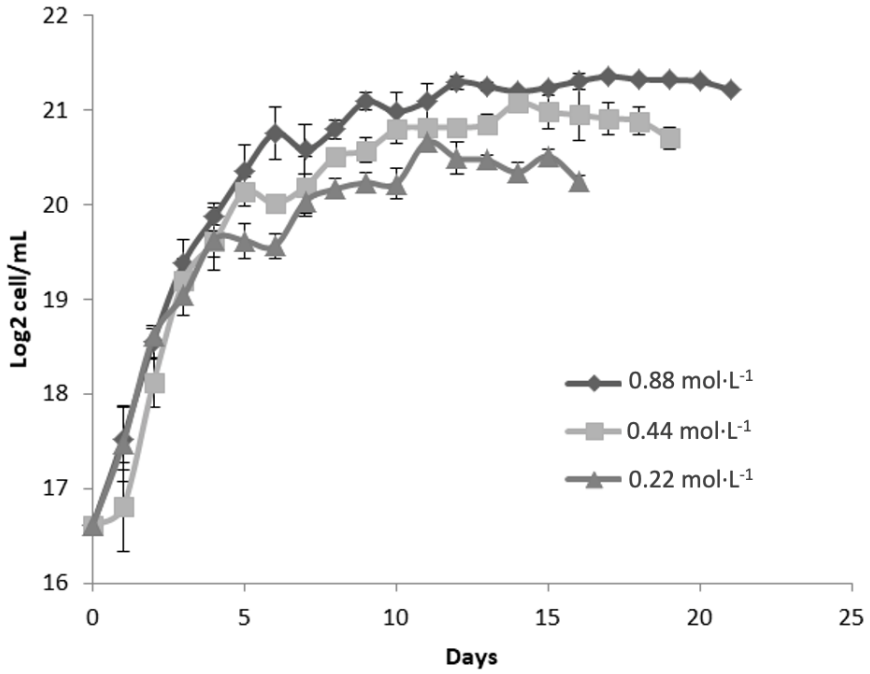


**Figure 3.** Growth kinetics (log2 cell/mL) of the microalgae Dunaliella tertiolecta at 45 PSU in different nitrogen concentrations (0.88 mol·L-1, 0.44 mol·L-1and 0.22 mol·L-1of NaNO3).

At the intermediate nitrogen level (0.44 mol·L$^{-1}$ $NaNO_3$), a similar growth trend was observed, though the maximum cell concentration was slightly lower than that of the 0.88 mol·L$^{-1}$ treatment. This suggests that moderate nitrogen supports cell proliferation but may not fully meet the elevated metabolic demands under high salinity. The lowest nitrogen concentration (0.22 mol·L$^{-1}$ $NaNO_3$) resulted in the poorest performance, with cultures reaching only ~19 $Log_2$ cell/mL and an earlier transition to stationary phase—signs of severe nitrogen limitation. The restricted nitrogen supply, combined with osmotic stress at 45 PSU, likely increased the metabolic burden, impairing protein synthesis, chlorophyll production, and division. Compared to 25 and 35 PSU (Figures 1 and 2), a progressive reduction in cell density was observed across all nitrogen levels as salinity increased. This trend underscores the negative impact of osmotic pressure on growth, as cells divert metabolic resources toward stress adaptation mechanisms like glycerol synthesis [31].

Despite the negative impact of high salinity on overall biomass yield, nitrogen supplementation at 0.88 mol·L$^{-1}$ appears to mitigate, at least partially, the growth inhibition associated with saline stress. This suggests that adequate nitrogen availability is essential not only for supporting basic metabolic functions but also for enabling osmoregulatory responses under extreme environmental conditions. These findings reinforce the critical role of nitrogen nutrition in the physiological performance of D. tertiolecta, particularly under high-salinity cultivation strategies commonly employed for the production of carotenoids and other high-value metabolites. Nitrogen limitation, while detrimental to biomass accumulation, is known to trigger the accumulation of secondary metabolites such as β-carotene due to stress-induced metabolic shifts. Therefore, the deliberate modulation of nitrogen supply in combination with salinity control could be strategically used to optimize either biomass production or metabolite enrichment, depending on the desired biotechnological outcome [33,34].

Growth kinetics analysis of Dunaliella tertiolecta under varying nitrogen and salinity conditions confirmed that both significantly affect cell proliferation and biomass [34]. The best outcome was observed at 25 PSU with 0.88 mol·L$^{-1}$ $NaNO_3$, where cultures entered stationary phase by day 7, maintaining the highest cell density. This suggests that harvesting at day 7 under these conditions is optimal for maximizing yield before nutrient depletion or loss of viability. These findings offer a valuable reference for optimizing D. tertiolecta cultivation when high biomass productivity is the target [34,35].

 doi:10.20944/preprints202508.0483.v1



*2.2. Optimizing Key Factors for the Biosynthesis of Chlorophyll a, b, and c*

The optimization of chlorophyll pigment production in Dunaliella tertiolecta was successfully evaluated through a Central Composite Design (CCD) matrix, considering nitrogen concentration ($X_1$), salinity ($X_2$), and culture age ($X_3$) as the independent variables. The responses analyzed included the concentrations of chlorophyll a ($C_a$), chlorophyll b ($C_\beta$), and chlorophyll c ($Cc_1+c_2$), expressed in mg/g of dry weight (dw). Both experimental responses and the predicted values obtained from the statistical model are presented in Table 1.

The results demonstrated significant variability in pigment production across the different experimental runs, highlighting the crucial influence of the tested factors and their interactions. The most remarkable pigment accumulation was observed in Run 10, where the nitrogen concentration was at its lowest level (0.22 mol·L$^{-1}$), salinity at 25 PSU, and culture age at 15 days. Under these conditions, the maximum experimental values for chlorophyll a (13.68 mg/g dw), chlorophyll b (4.85 mg/g dw), and chlorophyll c (3.71 mg/g dw) were recorded. The predicted responses by the model in this condition also showed high agreement with the experimental data (12.29 mg/g dw for $C_a$, 4.92 mg/g dw for $C_\beta$, and 3.41 mg/g dw for $Cc_1+c_2$), confirming the model's reliability and robustness in describing pigment production behavior under these specific conditions.

**Table 1.** Central Composite design matrix. Optimization of pigment production (Chlorophyll a, Chlorophyll b and Chlorophyll c) from microalgae D. tertiolecta.

| Run | Experimental variables | | | | Responses (mg/g *dw*) | | | Predicted responses (mg/g *dw*) | | |
|---|---|---|---|---|---|---|---|---|---|---|
| | Pattern | $X_1$ | $X_2$ | $X_3$ | $C_a$ | $C_b$ | $C_{c1+c2}$ | $C_a$ | $C_b$ | $C_{c1+c2}$ |
| 1 | 0A0 | 0.55 | 45 | 10 | 1.73 | 0.78 | 0.46 | 0.71 | 0.66 | 0.09 |
| 2 | 00a | 0.55 | 35 | 5 | 1 | 0.73 | 0.12 | 1.17 | 0.95 | 0.23 |
| 3 | a00 | 0.22 | 35 | 10 | 1.85 | 1.42 | 0.52 | 2.48 | 1.17 | 0.93 |
| 4 | -++ | 0.22 | 45 | 15 | 0.66 | 0.39 | 0.18 | 1.61 | 0.48 | 0.3 |
| 5 | 0a0 | 0.55 | 25 | 10 | 1.95 | 1.31 | 0.45 | 3.83 | 1.69 | 0.98 |
| 6 | 00A | 0.55 | 35 | 15 | 0.72 | 0.48 | 0.23 | 0.71 | 0.53 | 0.27 |
| 7 | 000 | 0.55 | 35 | 10 | 1.25 | 0.73 | 0.31 | 0.4 | 0.45 | 0.15 |
| 8 | ++- | 0.88 | 45 | 5 | 6.52 | 4.6 | 1.93 | 2.32 | 1.29 | 0.65 |
| 9 | +-+ | 0.88 | 25 | 15 | 2.38 | 1.77 | 0.77 | 2.71 | 1.54 | 0.83 |
| 10 | --+ | 0.22 | 25 | 15 | 13.68 | 4.85 | 3.71 | 12.29 | 4.92 | 3.41 |
| 11 | +-- | 0.88 | 25 | 5 | 4.41 | 2.24 | 1.02 | 3.25 | 2.08 | 0.86 |
| 12 | +++ | 0.88 | 45 | 15 | 2.88 | 1.28 | 0.56 | 2.32 | 1.29 | 0.65 |
| 13 | --- | 0.22 | 25 | 5 | 6.11 | 2.66 | 1.9 | 6.46 | 2.58 | 1.78 |
| 14 | A00 | 0.88 | 35 | 10 | 10 | 1.01 | 0.63 | 1.23 | 1.32 | 0.65 |
| 15 | -+- | 0.22 | 45 | 5 | 1.15 | 0.63 | 0.28 | 0.61 | 0.79 | 0.18 |

Experimental variables as the independent variables: $X_1$; nitrogen concentration (mol·L$^{-1}$ $NaNO_3$). $X_2$; Salinity (PSU). $X_3$; Culture age (days). Responses (mg/g dw) and Predicted responses (mg/g dw): $C_a$; Chlorophylle a. $C_b$; Chlorophylle a. $C_{c1+c2}$; Chlorophylle c.

The combination of low nitrogen availability and lower salinity appears to favor pigment accumulation, especially in later stages of cultivation. This is likely due to stress-induced metabolic responses in microalgae, where nitrogen limitation triggers carotenoid and chlorophyll synthesis as part of photoprotective and adaptive mechanisms [28,36]. In contrast, lower pigment levels were observed under higher nitrogen and salinity conditions at early harvest times. For instance, Run 2 (0.55 mol·L$^{-1}$ nitrogen, 35 PSU salinity, 5 days) showed significantly reduced chlorophyll yields (1.0

 doi:10.20944/preprints202508.0483.v1



mg/g dw for $C_a$, 0.73 mg/g dw for $C_\beta$, 0.12 mg/g dw for $Cc_1+c_2$). These results suggest that nitrogen sufficiency and short culture durations favor biomass growth over secondary metabolite production under non-stress conditions [37].

The model's predictive performance was validated by a non-significant lack-of-fit test ($p > 0.05$), confirming the adequacy of the quadratic polynomial equation in describing the relationship between factors and response variables. The close match between experimental and predicted values across most runs further supports the suitability of the CCD approach and the effectiveness of Response Surface Methodology (RSM) in modeling complex interactions. Data trends confirmed that nitrogen concentration, salinity, and culture age significantly influence pigment biosynthesis in D. tertiolecta. Specifically, nitrogen limitation combined with low to moderate salinity and extended culture duration proved most favorable for maximizing pigment yield. These findings offer valuable guidance for designing cultivation protocols to enhance pigment production in microalgae-based systems. Overall, the CCD design, supported by RSM analysis, proved effective for identifying optimal conditions and understanding environmental interactions affecting chlorophyll biosynthesis. This approach provides a solid framework for future applications in microalgal biotechnology, particularly for high-value pigment production [38,39].

The statistical evaluation of chlorophyll pigment production in Dunaliella tertiolecta using a Central Composite Design revealed distinct effects of nitrogen concentration, salinity, and light intensity, as well as their interactions, on the biosynthesis of chlorophylls a, b, and c. Analysis of variance (ANOVA) focused on the F value and significance level (Prob > F) to assess each factor's contribution to pigment accumulation. For chlorophyll a, nitrogen concentration ($X_2$) was the most significant factor ($F = 10.9196$, Prob > F = 0.0163**), indicating a clear effect at $p < 0.05$. The nitrogen–light interaction ($X_1 * X_3$) also showed significance ($F = 9.1295$, Prob > F = 0.0234**), while the nitrogen–salinity interaction ($X_1 * X_2$) had a highly significant effect ($F = 23.8088$, Prob > F = 0.0028*). These results underscore the importance of nitrogen availability and its interactions with salinity and light in modulating chlorophyll a biosynthesis in D. tertiolecta.

For chlorophyll b production, nitrogen concentration ($X_2$) was again the most influential factor, with an F value of 18.6571 and a highly significant Prob > F of 0.0050*. Significant quadratic effects were observed for both nitrogen ($X_2 * X_2$; $F = 9.8371$, Prob > F = 0.0202**) and salinity ($X_1 * X_1$; $F = 11.8230$, Prob > F = 0.0138**), indicating a non-linear response. The nitrogen–salinity interaction ($X_1 * X_2$) was highly significant ($F = 61.6937$, Prob > F = 0.0002*), confirming their synergistic role in regulating chlorophyll b levels. Additionally, the nitrogen–light interaction ($X_2 * X_3$) showed substantial significance ($F = 24.6091$, Prob > F = 0.0026*), suggesting that light modulates nitrogen's effect on chlorophyll b synthesis, likely via its role in photosystem regulation and nitrogen assimilation. For chlorophyll c, nitrogen concentration ($X_2$) remained a key determinant, with an F value of 12.4534 and a significant Prob > F of 0.0124**. The nitrogen–salinity interaction ($X_1 * X_2$) had the strongest effect ($F = 27.0237$, Prob > F = 0.0020*), highlighting its consistent importance across all chlorophyll types. Significant quadratic effects were also observed for salinity ($X_1 * X_1$; $F = 6.7666$, Prob > F = 0.0406**) and the nitrogen–light interaction ($X_2 * X_3$; $F = 7.2497$, Prob > F = 0.0359**), indicating a nonlinear response of chlorophyll c production to these environmental factors.

Overall, the ANOVA results across all three pigments consistently identify nitrogen concentration as the main factor driving chlorophyll biosynthesis in D. tertiolecta. However, significant interactions, particularly between nitrogen and salinity, and nitrogen and light, emphasize the relevance of combined environmental modulation over isolated effects. The significant quadratic terms indicate a complex, nonlinear relationship likely involving metabolic feedback and stress adaptation mechanisms. These findings align with the previously discussed growth kinetics, where higher nitrogen levels under optimal salinity favored biomass accumulation, providing a physiological basis for increased chlorophyll synthesis. This integrated analysis supports the targeted adjustment of cultivation conditions to enhance pigment production, with promising applications in nutraceutical and biotechnological fields [40].

 doi:10.20944/preprints202508.0483.v1



To support these findings and enable predictive modeling of pigment synthesis under varying culture conditions, mathematical modeling and statistical optimization were applied. Second-order polynomial equations were developed to more accurately estimate chlorophyll production and visualize factor interactions using response surface methodology. Predictive models for chlorophyll a, b, and c (Equations (1)–(3)) were generated with JMP V18 software, allowing estimation of pigment yields and construction of response surface plots. The predicted production ranges were 0.66–13.68 mg/g dw for chlorophyll a, 0.48–4.85 mg/g dw for chlorophyll b, and 0.12–3.71 mg/g dw for chlorophyll c.

*Eq. 1= 6.6687183908046 + (-1.8939393939394 * x1) + (-0.1559 * x2) + (0.0226 * x3) + ((x1-0.55) * (( x1-0.55) * 13.4083784554004)) + ((x1 – 0.55) * ((x2 – 35) * 0.77992424242424)) + ((x2 -35) * ((x2 – 35) * 0.01870172413793)) + ((x1 – 0.55) * ((x3 – 10) * -0.9659090909091)) + ((x2 – 35) * ((x3 – 10) * -0.024175)) + ((x3 – 10) * ((x3 – 10) * 0.03560689655172))*

*Eq. 2= 2.54573563218391 + (0.22424242424242 * x1) + (-0.0514 * x2) + (-0.0418 * x3) + ((x1 – 0.55) * ((x1 – 0.55) * 7.317691016675058)) + ((x1 – 0.55) * ((x2 – 35) * 0.31666666666667)) + ((x2 – 35) * ((x2 – 35) * 0.00726896551724)) + ((x1 – 0.55) * ((x3 – 10) * -0.4348484848485)) + ((x2 – 35) * ((x3 – 10) * -0.0132)) + ((x3 – 10) * ((x3 – 10) * 0.01167586206897))*

*Eq. 3= 1.90072413793104 + (-0.4272727272727 * x1) + (-0.0444 * x2) + (0.004 * x3) + ((x1 – 0.55) * ((x1 – 0.55) * 5.85320287514645)) + ((x1 – 0.55) * ((x2 – 35) * 0.22159090909091)) + ((x2 – 35) * ((x2 – 35) * 0.00382413793103)) + ((x1 – 0.55) * ((x3 – 10) * -0.2522727272727)) + ((x2 – 35) * ((x3 – 10) * -0.007575)) + ((x3 – 10) * ((x3 – 10) * 0.00409655172414))*

The second-order polynomial equations for chlorophyll a, b, and c production reveal how nitrogen concentration ($x_1$), salinity ($x_2$), and light intensity ($x_3$) influence pigment biosynthesis in Dunaliella tertiolecta. These models incorporate linear, quadratic, and interaction terms, enabling accurate prediction of pigment yields. For chlorophyll a (Eq. 1), the intercept value of 6.67 mg/g dw represents baseline production at central levels of the factors. Negative linear coefficients for nitrogen (-1.89) and salinity (-0.15) indicate that increasing these factors individually reduces chlorophyll a, while light intensity has a slight positive effect (0.02). A significant quadratic nitrogen term ($(x_1 – 0.55)^2 * 13.41$) suggests an optimal nitrogen level for maximum pigment yield. Interaction terms reveal synergistic effects between nitrogen and salinity ($(x_1 – 0.55)(x_2 – 35) * 0.78$) and antagonistic effects between nitrogen and light ($(x_1 – 0.55)(x_3 – 10) * -0.97$), underscoring the need to balance nutrients and stressors for optimal pigment production.

The predictive models for chlorophyll b (Equation (2)) and chlorophyll c (Equation (3)) reveal distinct regulatory patterns, highlighting the complexity of pigment synthesis in response to cultivation conditions. For chlorophyll b, the intercept (2.55 mg/g dw) reflects baseline production, with nitrogen showing a positive linear effect (0.22), unlike its negative effect on chlorophyll a—suggesting that moderate nitrogen levels may favor chlorophyll b synthesis. A significant quadratic nitrogen term ($(x_1 – 0.55)^2 * 7.32$) and interactions with salinity and light indicate nonlinear, cross-regulatory responses. For chlorophyll c, the intercept is 1.90 mg/g dw, with nitrogen showing a negative linear effect (-0.43), similar to chlorophyll a. However, quadratic and interaction effects—particularly nitrogen-salinity ($(x_1 – 0.55)(x_2 – 35) * 0.22$) and nitrogen-light ($(x_1 – 0.55)(x_3 – 10) * -0.25$)—play key roles, suggesting pigment production depends on both individual and combined factor effects. These models provide a valuable framework for optimizing pigment yields in microalgae-based bioprocesses.

### *2.3. Three-Dimensional Response Surface Modeling of Chlorophyll a, b, and c Production in Dunaliella tertiolecta*

The three-dimensional response surface plots presented in Figure 4 illustrate the predicted behavior of chlorophyll a, b, and c production in Dunaliella tertiolecta as a function of salinity (PSU) and culture age (days), with nitrogen concentration maintained at the central point of the experimental design. These models offer a comprehensive visualization of the curvature effects and

 doi:10.20944/preprints202508.0483.v1



interactive influence of the two independent variables on pigment biosynthesis, providing key insights into the physiological responses of the microalga under varying environmental conditions.

The response surface for chlorophyll a (Figure 4a) clearly shows that maximum pigment accumulation occurs at lower salinity levels combined with an extended cultivation period. The plot exhibits a convex curvature, where chlorophyll a production significantly increases with longer culture durations while remaining inversely correlated with salinity. This suggests that prolonged exposure to mild saline conditions facilitates the accumulation of chlorophyll a, likely due to the activation of adaptive stress responses that promote chlorophyll biosynthesis as part of the photosynthetic machinery reinforcement. At higher salinity levels, pigment accumulation decreases, probably due to osmotic stress, which can impair chloroplast integrity and photosystem stability, reducing the efficiency of chlorophyll synthesis [40].

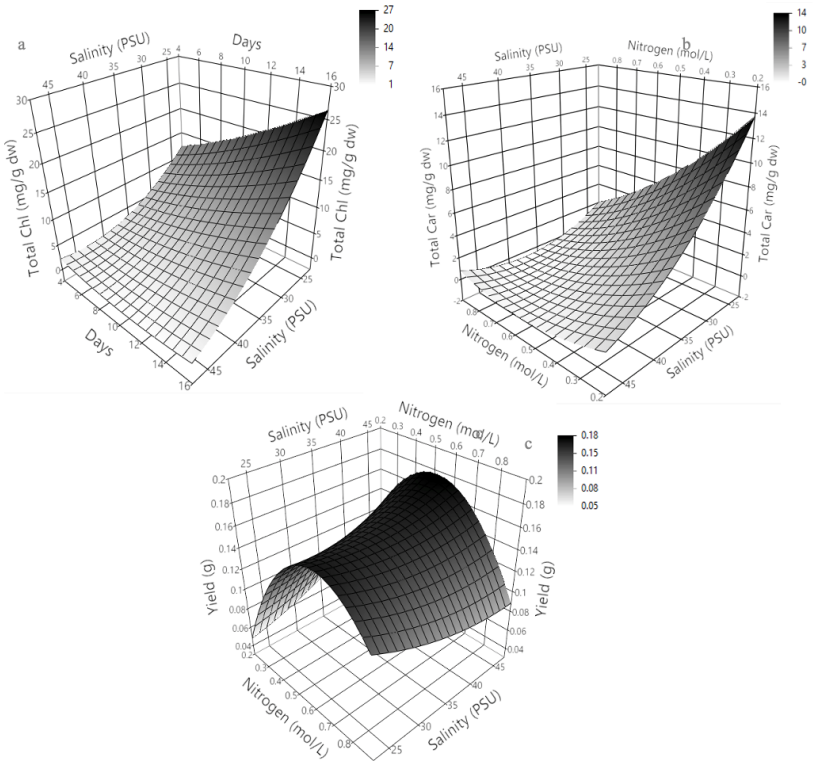


**Figure 4.** Tridimensional response surface representing chlorophyll a (a), chlorophyll b (b) and chlorophyll c (c) production (of the microalgae Dunaliella tertiolecta in function of salinity variation (PSU) and age of culture (harvest day) with nitrogen concentration (mol·L$^{-1}$ of NaNO3) as the central point.

Similarly, the surface response for chlorophyll b (Figure 4b) demonstrates a comparable trend, where the pigment yield improves under lower salinity and extended cultivation time. However, the curvature for chlorophyll b appears slightly less steep compared to chlorophyll a, indicating that chlorophyll b production is also sensitive to environmental stress but may exhibit different regulatory dynamics or stability under saline stress. This differential behavior could be attributed to the specific roles of chlorophyll b within the light-harvesting complexes (LHC II), which may allow partial maintenance of photosynthetic function even under moderate salinity. In the case of chlorophyll c (Figure 4c), the response surface shows a similar dependence on salinity and culture age, with the highest production observed at the lowest salinity and longest cultivation period tested. The plot highlights a gradual and continuous increase in chlorophyll c accumulation as salinity decreases and culture age increases, suggesting a sustained biosynthetic capacity of the algal cells for this pigment under prolonged non-stressful conditions. Chlorophyll c, being part of the peripheral antenna complexes in some algal groups, might play a photoprotective role or be involved in fine-tuning energy transfer under stress adaptation mechanisms.

 doi:10.20944/preprints202508.0483.v1



At the molecular level, these findings can be attributed to metabolic shifts triggered by nitrogen limitation and salinity stress, which modulate the transcription of chlorophyll biosynthetic enzymes like glutamyl-tRNA reductase and protochlorophyllide oxidoreductase. Prolonged culture under suboptimal salinity may redirect carbon fluxes toward pigment biosynthesis rather than biomass, increasing chlorophyll content per cell. These adaptive responses align with previous reports showing that environmental stress enhances pigment composition to optimize photosynthesis and protect against oxidative damage. The generated response surfaces confirm the significant roles of salinity and culture age in chlorophyll production and serve as predictive tools for optimizing cultivation. Adjusting these parameters enables maximum pigment yields in D. tertiolecta cultures, offering a strategic approach for nutraceutical or biotechnological applications. Overall, these results underscore the need to integrate environmental stress management with nutrient regulation to enhance pigment productivity in microalgal bioprocesses [41–43].

### *2.4. Optimizing Key Factors for theYield and Biosynthesis of Total Chlorophyll and Total Carotenoids*

The Central Composite Design (CCD) matrix presented in Table 2 provides a comprehensive evaluation of the effects of nitrogen concentration ($X_1$), salinity ($X_2$), and culture age ($X_3$) on total chlorophyll (T-Chl), total carotenoid (T-Car) content, and overall biomass yield in Dunaliella tertiolecta. The experimental results reveal significant variability in pigment production and yield across the 15 experimental runs, confirming the critical influence of the tested factors and their interactions. The highest total chlorophyll concentration (23 mg/g dw) and carotenoid content (13.26 mg/g dw) were achieved in Run 10, under conditions of low nitrogen (0.22 mol·L$^{-1}$), low salinity (25 PSU), and extended culture age (15 days). This result aligns with the previously discussed stress-induced enhancement of pigment biosynthesis, where nitrogen limitation and lower salinity trigger adaptive responses, redirecting metabolic fluxes toward secondary metabolite production rather than biomass accumulation.

Conversely, the lowest pigment concentrations were observed under high nitrogen and elevated salinity at early culture stages (e.g., Runs 2 and 4), where chlorophyll and carotenoid levels were reduced, indicating a prioritization of cell proliferation over pigment synthesis. Notably, higher pigment content did not always correlate with biomass yield, suggesting that pigment accumulation is more linked to stress adaptation than growth. For instance, Run 6 achieved the highest yield (0.166) but showed relatively low pigment levels, reflecting a trade-off between biomass formation and pigment biosynthesis. The predictive responses from the statistical model closely matched experimental values, validating the robustness of the quadratic equations and the CCD approach. This consistency, especially under high pigment-yielding conditions, confirms the model's effectiveness in capturing the complex interactions among nitrogen, salinity, culture age, and pigment production. These insights are key for optimizing D. tertiolecta cultivation strategies aimed at enhancing pigment output for nutraceutical, pharmaceutical, and biotechnological applications [43–45].

**Table 2.** Central Composite design matrix. Optimization of pigment production (total chlorophyll and total carotenoids) and yield from microalgae D. tertiolecta.

| Run | Experimental variables | | | | Responses (mg/g *dw*) | | | Predicted responses (mg/g *dw*) | | |
|---|---|---|---|---|---|---|---|---|---|---|
| | Pattern | $X_1$ | $X_2$ | $X_3$ | T-Chl | T-Car | Yield | T-Chl | T-Car | Yield |
| 1 | 0A0 | 0.55 | 45 | 10 | 3.07 | 0.99 | 0.133 | 2.10 | 0 | 0.13 |
| 2 | 00a | 0.55 | 35 | 5 | 1.89 | 0.11 | 0.1 | 2.91 | 0 | 0.10 |
| 3 | a00 | 0.22 | 35 | 10 | 3.83 | 1.19 | 0.065 | 6.72 | 2.43 | 0.05 |
| 4 | -++ | 0.22 | 45 | 15 | 1.26 | 0.72 | 0.108 | 3.6 | 1.73 | 0.12 |
| 5 | 0a0 | 0.55 | 25 | 10 | 3.74 | 0.86 | 0.1 | 7.66 | 2.68 | 0.10 |

 doi:10.20944/preprints202508.0483.v1



| | | | | | | | | | | |
|---|---|---|---|---|---|---|---|---|---|---|
| 6 | 00A | 0.55 | 35 | 15 | 1.48 | 0.53 | 0.166 | 3.42 | 1.38 | 0.16 |
| 7 | 000 | 0.55 | 35 | 10 | 2.34 | 0.76 | 0.101 | 2.43 | 0.07 | 0.11 |
| 8 | ++- | 0.88 | 45 | 5 | 13.35 | 2.78 | 0.023 | 15.35 | 4.59 | 0.02 |
| 9 | +-+ | 0.88 | 25 | 15 | 4.96 | 0.72 | 0.127 | 6.78 | 1.45 | 0.13 |
| 10 | --+ | 0.22 | 25 | 15 | 23 | 13.26 | 0.06 | 22.8 | 11.37 | 0.06 |
| 11 | +-- | 0.88 | 25 | 5 | 7.8 | 1.77 | 0.038 | 7.26 | 0.58 | 0.03 |
| 12 | +++ | 0.88 | 45 | 15 | 2.96 | 0.89 | 0.101 | 4.69 | 0.18 | 0.1 |
| 13 | --- | 0.22 | 25 | 5 | 11.04 | 3.55 | 0.018 | 11.11 | 4.08 | 0.02 |
| 14 | A00 | 0.88 | 35 | 10 | 5.28 | 0.46 | 0.028 | 5.34 | 0 | 0.04 |
| 15 | -+- | 0.22 | 45 | 5 | 2.12 | 0.62 | 0.1 | 2.1 | 0 | 0.1 |

Experimental variables as the independent variables: $X_1$; nitrogen concentration (mol·$L^{-1}$ $NaNO_3$). $X_2$; Salinity (PSU). $X_3$; Culture age (days). Responses (mg/g dw) and Predicted responses (mg/g dw): T-Chl; Total Chlorophylle . T-Car; Total carotenoids; Yield.

The statistical evaluation offers key insights into the effects and interactions influencing total chlorophyll, carotenoids, and biomass yield in Dunaliella tertiolecta under the CCD framework. Nitrogen concentration ($X_1$), salinity ($X_2$), and culture age ($X_3$) were assessed through F values and significance levels (Prob > F). For total chlorophyll, salinity ($X_2$) was the most significant factor (F = 17.4779, Prob > F = 0.0058*), emphasizing the impact of osmotic stress on pigment biosynthesis. Notably, the salinity–light ($X_2$ * $X_3$; F = 11.7467, Prob > F = 0.0140**) and nitrogen–light ($X_1$ * $X_3$; F = 16.7579, Prob > F = 0.0064*) interactions were significant, showing that pigment accumulation depends on combined environmental and nutritional conditions. The nitrogen–salinity interaction ($X_1$ * $X_2$; F = 33.1315, Prob > F = 0.0012*) also had a strong influence, suggesting that salinity can modulate nitrogen-driven chlorophyll synthesis. These findings highlight the need to simultaneously optimize multiple factors to maximize pigment yield.

Regarding total carotenoid production, salinity ($X_2$) once again demonstrated a significant linear effect (F = 6.1783, Prob > F = 0.0474**), while the nitrogen-salinity interaction ($X_1$ * $X_2$) showed a very strong influence (F = 10.9321, Prob > F = 0.0163**), reinforcing the evidence of interactive regulation between these two factors on pigment biosynthesis pathways. The nitrogen-culture age interaction ($X_1$ * $X_3$) was also statistically significant (F = 6.4316, Prob > F = 0.0443**), suggesting that the duration of cultivation plays a vital role in maximizing carotenoid production under specific nitrogen conditions. These results align with the known physiological mechanisms in microalgae where nitrogen limitation, combined with osmotic modulation and sufficient cultivation time, enhances the flux toward secondary metabolite pathways, particularly carotenoids, which function as antioxidants and photoprotective molecules.

For biomass yield, culture age ($X_3$) was the most influential factor (F = 55.0668, Prob > F = 0.0003*), indicating that longer cultivation significantly enhances biomass accumulation, consistent with typical microalgal growth patterns. The nitrogen–salinity interaction ($X_1$ * $X_2$) showed the highest F value among interactions (F = 25.1315, Prob > F = 0.0024*), highlighting the critical role of balancing nutrients and salinity for optimal productivity. A significant quadratic effect of nitrogen ($X_1$ * $X_1$; F = 73.4496, Prob > F = 0.0001*) revealed a nonlinear relationship, where both low and high nitrogen levels can impair growth. Additionally, the nitrogen–culture age interaction ($X_1$ * $X_3$; F = 11.7652, Prob > F = 0.0140**) and the quadratic term for culture age ($X_3$ * $X_3$; F = 9.4601, Prob > F = 0.0218**) were significant, suggesting that biomass yield depends on a precise combination of nutrient input and cultivation time to avoid growth limitations or inefficiencies.

Collectively, these findings provide robust statistical evidence that pigment production and biomass yield in D. tertiolecta are modulated not only by individual cultivation parameters but also by their interactions, supporting the need for an integrative optimization strategy. These results confirm the effectiveness of the CCD approach and response surface methodology as predictive tools

 doi:10.20944/preprints202508.0483.v1



for optimizing pigment production and biomass yield in microalgal cultivation, enabling the strategic design of efficient bioprocesses [45]. To support these findings and generate predictive models, second-order polynomial equations were developed using JMP V11. This enabled precise estimation of response variables and visualization of factor interactions via response surface methodology. The predicted ranges were 1.26–23 mg/g dw for total chlorophyll (Equation (4)), 0.11–13.26 mg/g dw for carotenoids (Equation (5)), and 0.018–0.133 g for yield (Equation (6)).

*Eq. 4= 12.7978965517241 + (-2.0909090909091 * x1) + (-0.2778 * x2) + (0.0508 * x3) + ((x1 – 0.55) * ((x1 – 0.55) * 33.0546847788227)) + ((x1 – 0.55) * ((x2 – 35) * 1.29583333333333)) + ((x2 – 35) * ((x2 – 35) * 0.02449655172414)) + ((x1 – 0.55) * ((x3 – 10) * -1.8431818181818)) + ((x2 – 35) * ((x3 – 10) * -0.050925)) + ((x3 – 10) * ((x3 – 10) * 0.02918620689655))*

*Eq. 5= 5.65984482758621 + (-3.8272727272727 * x1) + (-0.1407 * x2) + (0.144 * x3) + ((x1 – 0.55) * ((x1 – 0.55) * 10.09626040974)) + ((x1 – 0.55) * ((x2 – 35) * 0.63409090909091)) + ((x2 – 35) * ((x2 – 35) * 0.01199482758621)) + ((x1 – 0.55) * ((x3 – 10) * -0.9727272727273)) + ((x2 – 35) * ((x3 – 10) * -0.02635)) + ((x3 – 10) * ((x3 – 10) * 0.02377931034483))*

*Eq. 6= 0.01347011494253 + (-0.010303030303 * x1) + (0.00122 * x2) + (0.00566 * x3) + ((x1 – 0.55) * ((x1 – 0.55) * -0.584528672303)) + ((x1 – 0.55) * ((x2 – 35) * -0.0064772727273)) + ((x2 – 35) * ((x2 – 35) * 0.00006344827586)) + ((x1 – 0.55) * ((x3 – 10) * 0.00886363636364)) + ((x2 – 35) * ((x3 – 10) * -0.0001125)) + ((x3 – 10) * ((x3 – 10) * 0.00091379310345))*

The second-order polynomial equations for total chlorophyll (Equation (4)), total carotenoids (Equation (5)), and biomass yield (Equation (6)) offer a solid framework for predicting these responses under different cultivation conditions. Each model includes linear, quadratic, and interaction terms, capturing the complex effects of nitrogen concentration ($x_1$), salinity ($x_2$), and culture age ($x_3$). For total chlorophyll (Equation (4)), the intercept (12.80 mg/g dw) represents baseline production under central conditions. Negative linear coefficients for nitrogen (-2.09) and salinity (-0.28) suggest that higher values reduce chlorophyll synthesis, while the positive effect of culture age (0.05) indicates that longer cultivation favors pigment accumulation. The significant nitrogen quadratic term ($(x_1 – 0.55)^2 * 33.05$) reveals a strong curvature, pointing to an optimal nitrogen level. Interaction effects—particularly between nitrogen and salinity (1.29), and nitrogen and culture age (-1.84)—highlight the importance of combined optimization, as these variables can act synergistically or antagonistically in modulating chlorophyll biosynthesis.

Equation (5) for total carotenoids follows a similar structure to chlorophyll but reveals distinct factor influences. The intercept (5.66 mg/g dw) sets the baseline, with nitrogen showing a strong negative linear effect (-3.83) and culture age a moderate positive effect (0.14), indicating that nitrogen limitation and prolonged cultivation promote carotenoid accumulation, likely as a stress response. The significant quadratic nitrogen term ($(x_1 – 0.55)^2 * 10.10$) confirms a nonlinear behavior with an optimal nitrogen level. Interactions—particularly nitrogen–salinity (0.63) and nitrogen–culture age (-0.97)—also influence carotenoid biosynthesis. For biomass yield (Equation (6)), the intercept is 0.0135 g. Nitrogen negatively affects yield (-0.0103), while salinity (0.00122) and culture age (0.00566) contribute positively. The nitrogen quadratic term ($(x_1 – 0.55)^2 * -0.58$) suggests yield decreases at extreme nitrogen levels. Although interaction effects are smaller, they confirm that yield depends on the combined influence of all factors. These models enable strategic optimization in microalgal bioprocesses.

The analysis of the Central Composite Design (CCD) and statistical modeling showed that total chlorophyll, carotenoid production, and biomass yield in Dunaliella tertiolecta are significantly influenced by the interactions between nitrogen concentration, salinity, and culture age. ANOVA results identified salinity and culture age as key for chlorophyll and biomass, while nitrogen, especially under limitation, strongly affected carotenoids. Significant quadratic and interaction terms confirmed the system's nonlinear nature, indicating that optimal pigment and biomass levels require balancing all variables rather than adjusting one in isolation [43–45]. These findings align with known stress responses in microalgae, where nitrogen limitation and osmotic stress enhance secondary metabolite pathways as adaptive mechanisms.

 doi:10.20944/preprints202508.0483.v1



*2.5. Three-Dimensional Response Surface Modeling of Total Chlorophyll, Total Carotenoids Production and Microalgal Biomass Yield in Dunaliella tertiolecta*

The three-dimensional response surface plots presented in Figure 5 illustrate the predictive modeling of total chlorophyll (Figure 5a), total carotenoids (Figure 5b), and biomass yield (Figure 5c) in Dunaliella tertiolecta, providing a comprehensive view of how these responses are influenced by variations in salinity (PSU), culture age (days), and nitrogen concentration (mol·L$^{-1}$ $NaNO_3$). These plots, generated from the second-order polynomial equations derived through the Central Composite Design (CCD), effectively capture the curvature and interactive effects between the evaluated parameters, offering valuable insights into the physiological behavior and metabolic regulation of this microalga under different cultivation conditions.

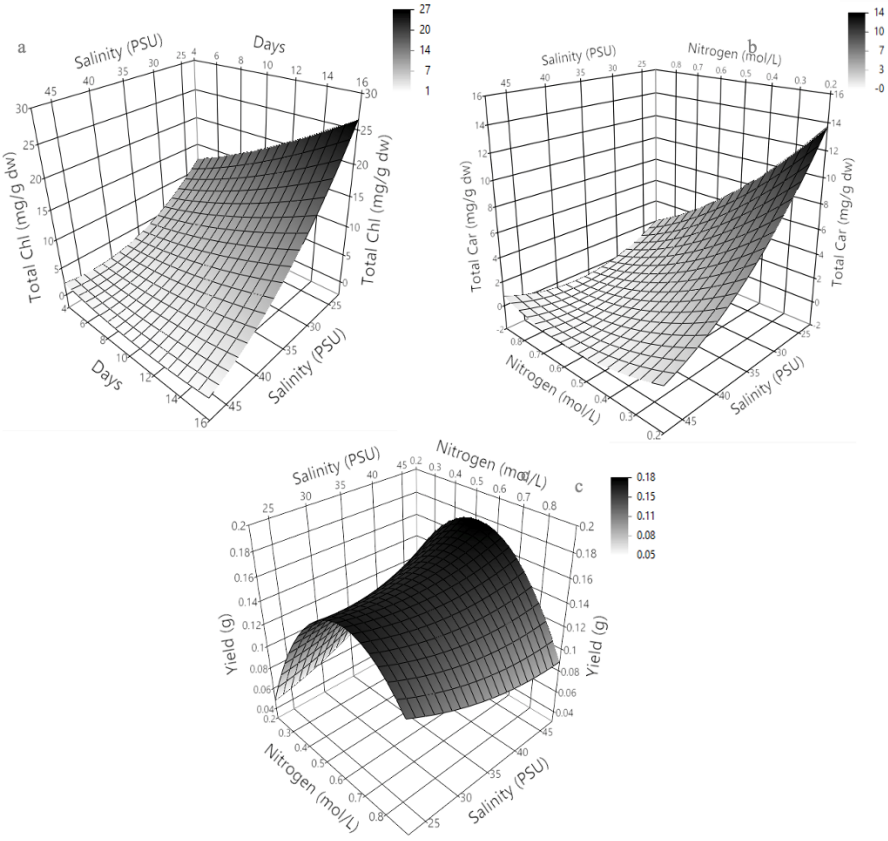


**Figure 5.** Tridimensional response surface representing total chlorophyll, carotenoids and yields production of the microalgae Dunaliella tertiolecta in function of nitrogen concentration (mol·L$^{-1}$ of $NaNO_3$) and salinity variation (PSU) on day 15 (5a); nitrogen concentration and age of culture (days) at 25 PSU (5b) and salinity and age of culture with 0.22 mol·L$^{-1}$ of $NaNO_3$ (5c).

The response surface analysis for total chlorophyll (Figure 5a) and total carotenoids (Figure 5b) in Dunaliella tertiolecta highlights the critical influence of salinity, culture age, and nitrogen concentration on pigment biosynthesis. Chlorophyll accumulation increases with extended cultivation and decreases with higher salinity, reaching maximum levels at low salinity (~25 PSU) and long culture durations (~15 days). This suggests that mild osmotic stress and prolonged growth favor chlorophyll production as part of the cell's adaptive response, likely mediated by the upregulation of biosynthetic enzymes under nitrogen limitation and low salinity to optimize light capture. Similarly, carotenoid production follows this trend but shows greater sensitivity to nitrogen levels. Peak carotenoid accumulation occurs at low salinity and reduced nitrogen, supporting the role of nitrogen deprivation as a strong inducer of secondary carotenoid biosynthesis. The nonlinear curvature of the response surface confirms that carotenoid production declines at higher nitrogen levels, even under optimal salinity, due to a metabolic shift toward growth rather than stress-related

 doi:10.20944/preprints202508.0483.v1



metabolite synthesis. These findings align with known stress-response mechanisms in microalgae, where nitrogen limitation redirects metabolism toward antioxidant and photoprotective pigment production, enhancing cellular defense under unfavorable conditions.

The response surface for biomass yield (Figure 5c) reveals a distinct pattern, with maximum yield achieved at moderate nitrogen concentrations and intermediate salinity, while culture age has a lesser impact. Unlike pigment accumulation, which benefits from nitrogen limitation and low salinity, these stress conditions reduce biomass growth, highlighting a metabolic trade-off between proliferation and secondary metabolite production. The peak yield near the central nitrogen level indicates that sufficient nitrogen is essential for cell growth, whereas excessive limitation hinders biomass despite enhancing pigment synthesis. These models illustrate the complex regulation of pigment and biomass production in D. tertiolecta, shaped by the interplay of salinity, nitrogen, and culture duration. The findings confirm the utility of the CCD approach and response surface methodology in predicting outcomes and offer practical strategies to optimize cultivation—whether aiming to increase pigment content for nutraceutical use or biomass for bioresource applications—by adjusting environmental conditions according to specific production goals [40].

The optimization of cultivation parameters using Central Composite Design and response surface methodology identified nitrogen concentration, salinity, and culture age as key factors influencing pigment biosynthesis and biomass yield in Dunaliella tertiolecta [38–40]. Optimal pigment production—23 mg/g dw of chlorophyll and 13.26 mg/g dw of carotenoids—was achieved under low nitrogen (0.22 mol·$L^{-1}$ $NaNO_3$), low salinity (25 PSU), and extended culture (15 days), as shown in Run 10. These conditions promote a stress-induced metabolic shift toward secondary metabolite accumulation while maintaining acceptable biomass yield. In contrast, higher nitrogen levels enhanced biomass but suppressed pigment synthesis, confirming a trade-off between growth and pigment production. Thus, the selected conditions strategically favor high-value pigment output for biotechnological applications. All subsequent analyses, including pigment encapsulation into nanoliposomes and their physicochemical characterization, will use biomass from this optimized condition to ensure consistency and relevance in evaluating the developed delivery systems.

### *2.6. High-Performance Liquid Chromatography (HPLC) of Pigment-Richt Optimized Microalgae Extract*

The HPLC chromatogram presented in Supplementary material 1 and Table 3 shows the pigment profile of the Dunaliella tertiolecta extract, obtained at a detection wavelength of 457 nm, which is characteristic for carotenoids due to their strong absorbance in the blue region of the visible spectrum. The chromatographic separation revealed seven distinct peaks, each corresponding to different pigments present within the extract. The early retention peaks (particularly peaks 1 and 2) likely represent more polar carotenoids such as all-trans violaxanthin and 13-cis lutein, which generally elute earlier due to their hydroxylated structures increasing polarity. All-trnas-violaxanthin is the pigment more abundant in the Dunaliella tertiolecta extarct. Peaks 3 may correspond to mono-epoxy carotenoid (all-trans luteoxanthin), which are commonly found in microalgal pigment profiles. Peak 4 is all-trans zeaxanthin which according to bibliographic references, is common in microalgae [46]. The last peaks (5- 7) are characteristic of less polar carotenoids as all-trans $\alpha$-carotene, all-trans $\beta$-carotene and 9-cis-$\beta$-carotene. The latter is one of the most abundant carotenoids reported in Dunaliella species, particularly under nitrogen limitation or stress conditions where $\beta$-carotene accumulation is enhanced [46,47]. Similar results are obtained by some references [48,49]. Unfortunately some peaks could not be identified, representing a quantification of 6.79%.

**Table 3.** Pigment profile of Dunaliella tertiolecta extract by HPLC at 457 nm.

| Peak | Name | Retention time (min) | Relative abundance (%) |
|---|---|---|---|
| 1 | all-trans violaxanthin | 1.65 | 45.16 |

 doi:10.20944/preprints202508.0483.v1



| | | | |
|---|---|---|---|
| 2 | 13-cis lutein | 2.12 | 0.5 |
| 3 | all-trans luteoxanthin | 2.98 | 2.7 |
| 4 | all-trans zeaxanthin | 4.01 | 2.43 |
| 5 | all-trans $\alpha$-carotene | 5.52 | 3.6 |
| 6 | all-trans β-carotene | 6.25 | 4.5 |
| 7 | 9-cis-β-carotene | 9.08 | 34.32 |

Structurally, β-carotene is a highly conjugated polyene hydrocarbon with no oxygen-containing functional groups, which contributes to its non-polar nature and its later elution in reverse-phase HPLC systems. Extensive π-conjugation systems facilitate strong light absorption. This behavior contrasts with other xanthophyll carotenoids (such as lutein and violaxanthin) that contain hydroxyl or epoxy groups, increasing their polarity and resulting in earlier retention times.

The presence of β-carotene in the D. tertiolecta extract aligns with the known metabolic pathways of this species, where the carotenoid biosynthesis involves enzymes such as phytoene synthase, lycopene cyclase, and β-carotene hydroxylase. Under stress conditions like high light intensity or nutrient deprivation, the expression of these enzymes is modulated, leading to the preferential accumulation of β-carotene as a photoprotective strategy. This molecular adaptation not only supports light harvesting and reactive oxygen species quenching but also explains the dominance of β-carotene in the pigment profile, as evidenced by the one of the major peaks observed in the chromatogram *[46–49]*.

Although all-trans violaxanthin was the major compound in the D. tertiolecta extract, β-carotene has some advantages over this compound. β-carotene is a precursor of vitamin A, essential for vision, immunity, and growth. Violaxanthin does not have significant provitamin A activity. Furthermore, β-carotene is generally more stable to heat and light compared to violaxanthin, which contains labile epoxides. Furthermore, β-carotene is widely approved as an additive (E160a) by the FDA (Food and Drug Administration) and EFSA (European Food Safety Authority); it is used in beverages, snacks, and supplements. Violaxanthin is not as widely regulated. Although both have antioxidant activity, β-carotene effectively neutralizes lipophilic free radicals, making it more versatile in biological systems [6]. Therefore, β-carotene is superior to violaxanthin in many contexts, highlighting its provitamin A activity, stability, bioavailability, and industrial and nutritional applications. Consequently, the interest in its placement in nanoliposomes improves its stability against oxidation and light, increases its bioavailability and intestinal absorption, and allows for controlled and targeted release in nutraceutical applications [15]. Furthermore, this technology protects its antioxidant activity and enhances its physiological effects [11,20,22,50].

### *2.7. Nano-Sized Liposomes via Particle Dispersion Method*

The extract from the optimized microalgal biomass (0.22 mol·L$^{-1}$ $NaNO_3$; 25 PSU; 15 days) and the β-carotene (food-grade by Sigma-Aldrich Co.) were encapsulated in nano-liposomal vehicles composed of phosphatidylcholine and cholesterol using the particle dispersion method. A final volume of 100 mL of each nano-liposomal vehicles loaded and suspended in saline solution was obtained, which were stored in freezing conditions and darkness until the lyophilization process. Once lyophilized, the yielding was 245 mg of nano-liposomes loaded with microalgal extract (Figure 6A), and 260 mg of nano-liposomes loaded with β-carotene (Figure 6B).

 doi:10.20944/preprints202508.0483.v1



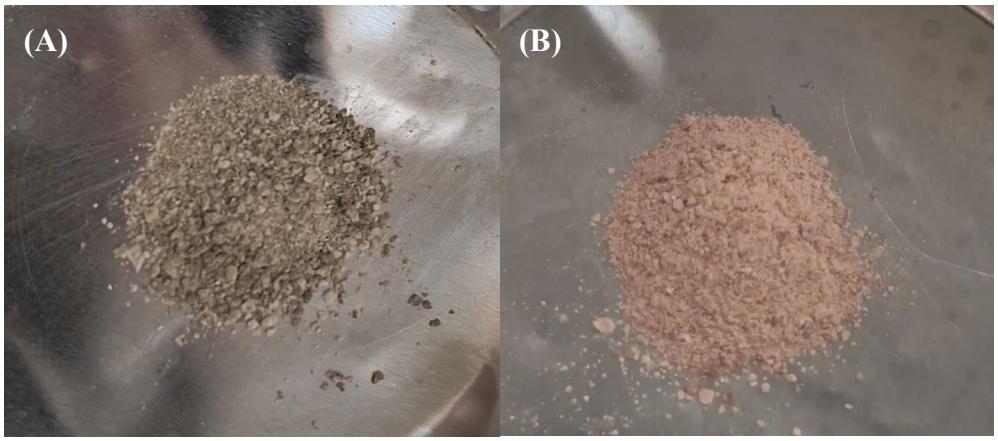


**Figure 6.** Microalgae extract-loaded nanoliposome (A) and β-carotene-loaded nanoliposome (B).

*2.8. Encapsulation Efficiency*

The encapsulation efficiency results revealed notable differences between the nanoliposomes loaded with Dunaliella tertiolecta extract and those containing pure β-carotene. Specifically, nanoliposomes encapsulating the microalgal extract exhibited an encapsulation efficiency of 43.45 ± 3.23%, whereas nanoliposomes loaded with β-carotene alone achieved a significantly higher efficiency of 94.67 ± 3.56%. This discrepancy may be attributed to the compositional complexity and structural diversity of the extract, which includes a mixture of seven carotenoids, namely, all-trans violaxanthin, 13-cis lutein, all-trans luteoxanthin, all-trans zeaxanthin, all-trans $\alpha$-carotene, all-trans β-carotene, and 9-cis-β-carotene, as identified by HPLC analysis *[46–49]*. These structurally diverse compounds, differing in polarity, isomeric configuration, and degree of unsaturation, may compete for integration into the liposomal bilayer or be less compatible with the hydrophobic core, thus limiting their encapsulation efficiency. Moreover, certain xanthophylls such as violaxanthin and luteoxanthin possess polar functional groups that may disrupt optimal incorporation into the lipid bilayer, causing a partial exclusion from the vesicular system or association with the vesicle surface rather than complete entrapment within the core [50,51].

At the interactional molecular level, β-carotene's superior encapsulation can be explained by its highly hydrophobic, planar, and symmetric polyene structure, which facilitates its stable incorporation into the hydrophobic region of the phospholipid bilayer. The extended system of conjugated double bonds allows for favorable van der Waals interactions and π-π stacking with the acyl chains of the phospholipids, contributing to its thermodynamic compatibility with the lipid environment. In contrast, the carotenoid mixture in D. tertiolecta extract introduces steric hindrance, varying degrees of polarity, and cis-isomerization that may reduce the efficiency of entrapment. Additionally, possible competitive interactions between carotenoids in the extract and the lipid headgroups or aqueous interface may further limit encapsulation. These molecular dynamics highlight the importance of compound-lipid compatibility and the physicochemical nature of bioactives when designing nanocarrier systems for complex natural extracts [52].

*2.9. Centrifugal Stability Measurement*

The centrifugal stability measurement revealed a significant difference between the two nanoliposomal formulations: β-CAR-LN exhibited a high stability of 87.75 ± 2.38%, while Dt-LN showed a markedly lower stability of 38.76 ± 3.64%. This disparity reflects the intrinsic chemical and structural differences between the encapsulated compounds and their molecular interactions with the liposomal bilayer. β-carotene, being a highly hydrophobic molecule with a linear, symmetric polyene chain, exhibits excellent compatibility with the hydrophobic core of the phospholipid bilayer. Its uniform structure facilitates deep insertion and strong van der Waals and π–π stacking interactions with the acyl chains of the phospholipids, leading to a compact, well-integrated liposomal structure with minimal leakage during centrifugation. In contrast, the Dunaliella tertiolecta

 doi:10.20944/preprints202508.0483.v1



extract (Dt-LN) contains a heterogeneous mixture of seven structurally diverse carotenoids, including polar xanthophylls (e.g., violaxanthin and luteoxanthin), and both cis and trans isomers. These molecules differ in polarity, isomeric configuration, and functional groups, which can disrupt the lipid packing of the bilayer, reducing vesicle integrity and promoting phase separation or surface localization of some compounds. The lower centrifugal stability of Dt-LN correlates with its low encapsulation efficiency (43.45%), indicating that a significant portion of the extract remains weakly associated with the lipid interface or exists outside the vesicles. Structurally, the presence of bulky, oxygenated carotenoids may create steric hindrance and limit their incorporation into the hydrophobic bilayer, resulting in poor physical stability under centrifugal stress. This compromised stability could lead to premature release or degradation of bioactives, thereby reducing the functional efficacy of the nanocarrier system. Conversely, the high stability of β-CAR-LN aligns with its high encapsulation efficiency (94.67%), confirming the importance of molecular compatibility in ensuring both efficient loading and structural robustness of nanoliposomes. These results highlight the necessity of tailoring the lipid composition and encapsulation strategy based on the physicochemical nature of the encapsulated compounds to achieve optimal performance in delivery systems [53].

*2.10. In Vitro Release*

The in vitro release kinetics of both the *Dunaliella tertiolecta* extract and pure β-carotene from nanoliposomes revealed distinct behaviors associated with their molecular structure and compatibility with the lipid bilayer (Figure 7). The release profile of the *D. tertiolecta* extract showed a gradual increase in concentration over time, reaching a cumulative release of approximately 390 µg/mL after 24 hours. In contrast, β-carotene exhibited a more sustained and higher release, reaching up to 891 µg/mL under the same conditions. These results correlate with their respective encapsulation efficiencies, 43.45% for the *D. tertiolecta* extract and 94.67% for β-carotene, and confirm that compounds with higher affinity to the liposomal core are released in a more controlled and efficient manner. Structurally, β-carotene is a highly hydrophobic molecule with a linear, symmetric polyene chain, which allows deep insertion into the hydrophobic region of the liposomal membrane. This results in strong van der Waals and π–π stacking interactions with phospholipid acyl chains, stabilizing the encapsulation and facilitating a gradual diffusion-based release [53].

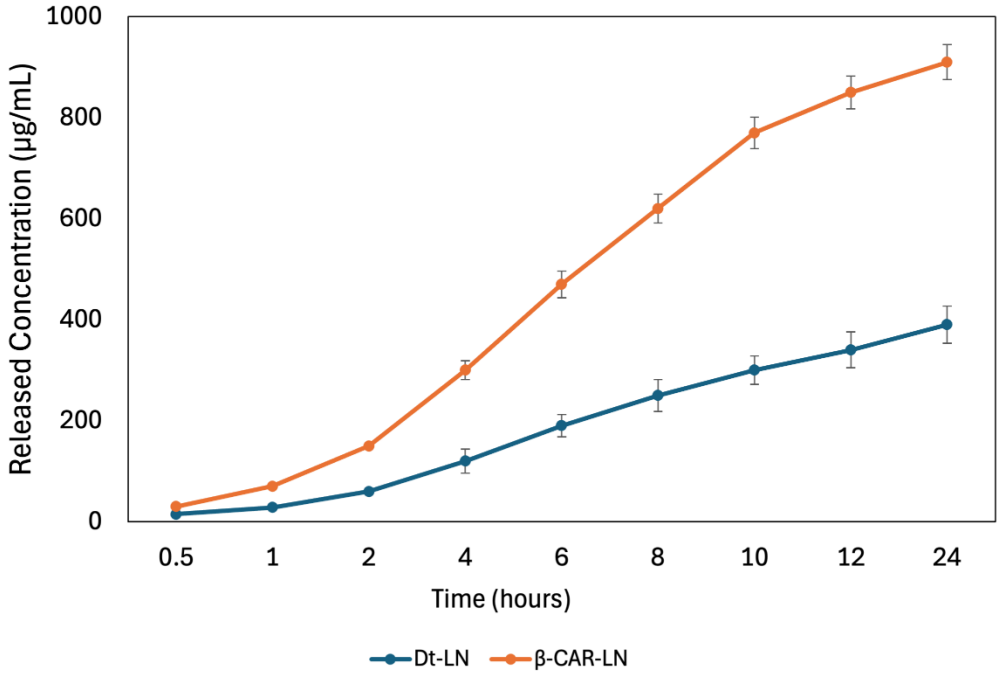


**Figure 7.** In vitro release profiles of *Dunaliella tertiolecta* extract (Dt-LN) and pure β-carotene (β-CAR-LN) from nanoliposomes over a 24-hour period. The released concentration (µg/mL) was measured at predetermined time intervals.

 doi:10.20944/preprints202508.0483.v1



The Korsmeyer-Peppas model was applied to describe the release mechanisms, yielding an exponent $n$= 0.611 for the *D. tertiolecta* extract and $n$= 0.585 for β-carotene, with corresponding release rate constants $k$ of 0.161 and 0.181, respectively (Figure 8). These values suggest that both systems follow a non-Fickian (anomalous) transport mechanism, where the release is governed by a combination of diffusion through the lipid matrix and structural relaxation or erosion of the liposomal bilayer. The model's fit was strong for both formulations, with $R^2$ values of 0.926 for the *D. tertiolecta* extract and 0.898 for β-carotene, indicating that the kinetic model adequately captures the release behavior. The slightly higher $R^2$ for the extract implies a better predictability of the model in more complex mixtures, despite its lower encapsulation and stability. This may be due to the presence of polar carotenoids (such as violaxanthin and luteoxanthin) that preferentially localize at the lipid–aqueous interface and are released earlier, while less polar carotenoids like β-carotene remain embedded and are released more slowly. Collectively, these findings emphasize the critical role of compound–lipid compatibility in determining both the stability and release dynamics of nanoliposomal delivery systems. This type of analysis is crucial for optimizing controlled-release formulations in nutraceutical or pharmaceutical applications [54].

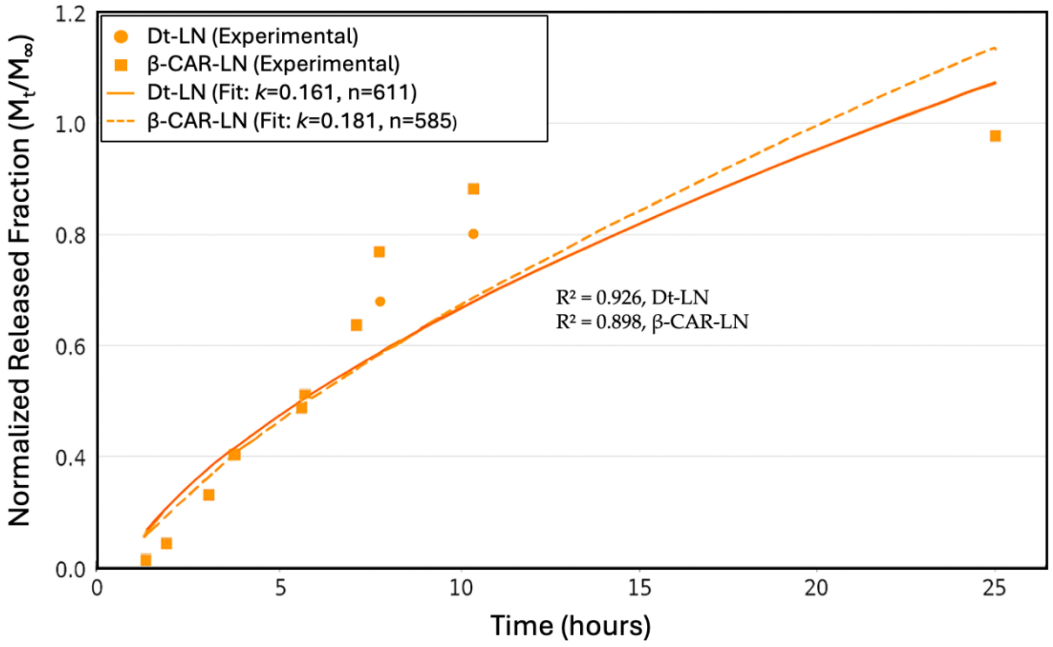


**Figure 8.** Korsmeyer-Peppas kinetic model fitting describing the in vitro release of *Dunaliella tertiolecta* extract and β-carotene from nanoliposomes. The normalized released fraction (Mt/M∞) was plotted as a function of time, showing anomalous release kinetics for both systems. Experimental data fitted the model with high correlation, indicating a combined mechanism of diffusion and lipid matrix relaxation. $M_t$ = Amount of compound released at time t; $M_\infty$: total amount released at equilibrium (∞); $k$= kinetic constant (related to the release rate); $n$= release exponent (indicates the transport mechanism). $R^2$ = Represents the goodness of fit (coefficient of determination).

*2.8. Sustained-Release Kinetics and Antioxidant Activities of Loaded Nanoliposomes*

The ABTS•⁺ and FRAP assays were used to evaluate the antioxidant activity of the pigment-loaded nanoliposomes. Prior to the assays, 20 mg of the lyophilized samples were resuspended in 10 mL of physiological solution (0.9% sodium chloride) for each test. Absorbance measurements were taken at 0, 15, 30, and 45 minutes, as well as from 1 to 8 hours as shown in Figures 9 and 10.

2.8.1. ABTS Assay

The results shown in Figure 9 illustrate the sustained release kinetics and antioxidant activity of nanoliposomes loaded with the optimized microalgal extract (Dt-LN) and β-carotene (β-CAR-LN),

 doi:10.20944/preprints202508.0483.v1



evaluated by the ABTS•⁺ radical scavenging assay and expressed in μmol TE/g over a period of 8 hours. Both nanoformulations demonstrated a controlled and gradual release profile, with a progressive increase in antioxidant activity throughout the evaluated time, suggesting effective encapsulation and sustained delivery of bioactive compounds. Initially, within the first hour, both systems exhibited a slight decrease in ABTS•⁺ inhibition, likely due to the stabilization phase of the nanoliposomes in the release medium, followed by a steady recovery and gradual increase in antioxidant potential. This initial dip may also reflect a rapid release of surface-associated compounds before the controlled release from the nanoliposomal core becomes dominant [55]. The highest antioxidant activities were recorded after 8 hours of exposure to the physiological solution, yielding values of 10.79 ± 0.15 and 10.90 ± 0.18 μmol TE/g for nanoliposomes loaded with *Dunaliella tertiolecta* extract and β-carotene, respectively. A comparable trend was observed in the FRAP assay, with values of 7.93 ± 1.12 and 8.14 ± 0.81 μmol TE/g for nanoliposomes encapsulated with *D. tertiolecta* extract and β-carotene, respectively.

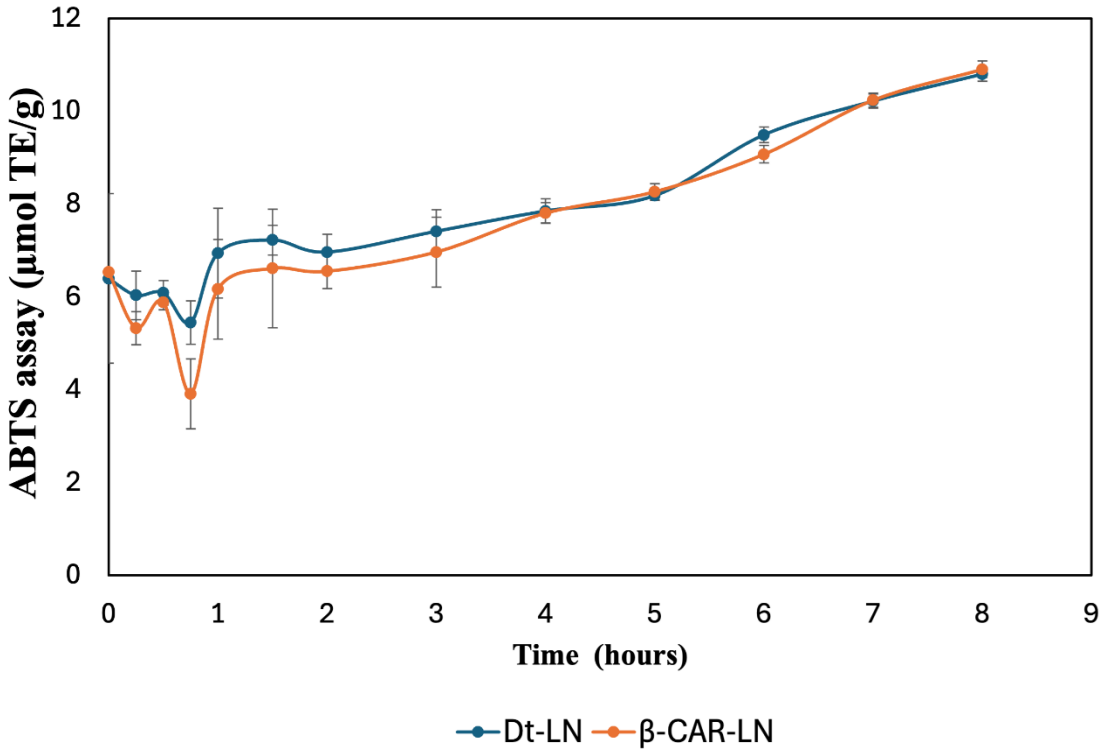


**Figure 9.** Sustained-release kinetics of the nano-liposomes loaded with microalgal extract and β-carotene on ABTS•⁺.

The Dt-LN formulation consistently showed slightly higher antioxidant activity than β-CAR-LN, especially during the early to intermediate release phases (1–6 hours). This suggests that the microalgal extract, containing a diverse mix of chlorophylls, carotenoids, and other antioxidants, may exert synergistic effects that enhance radical scavenging beyond β-carotene alone [51–53]. The structural diversity of both polar and non-polar compounds likely contributes to broader antioxidant action. The sustained release observed is linked to the nanoliposome's bilayer structure, which gradually releases encapsulated compounds through a semi-permeable phospholipid matrix. Hydrophobic molecules like carotenoids and chlorophylls diffuse slowly through this lipid barrier. Additionally, interactions between bioactives and the lipid matrix influence release rates, with β-carotene's stronger affinity for the hydrophobic core leading to a slightly slower release than the more complex Dt-LN mixture [54–57].

In the later stages of the kinetic profile (after 6 hours), both Dt-LN and β-CAR-LN formulations reached similar antioxidant activity levels, indicating that most encapsulated compounds had been released, allowing full interaction with ABTS•⁺ radicals. This plateau confirms the nanoliposomal

 doi:10.20944/preprints202508.0483.v1



system's effectiveness in sustaining antioxidant release over time—an important feature for applications in functional foods, nutraceuticals, and therapeutics. The overall results validate nanoliposomal encapsulation as a reliable strategy for prolonged delivery of antioxidant compounds from both microalgal extract and β-carotene. Notably, the superior early performance of Dt-LN underscores the benefits of complex natural extracts, which offer synergistic interactions, and a broader antioxidant spectrum compared to isolated compounds. This sustained release behavior may enhance oxidative protection in biological systems, increasing the functional and bioactive potential of the encapsulated compounds [58–60].

2.8.2. FRAP Assay

The results presented in Figure 11 depict the sustained-release kinetics and ferric reducing antioxidant power (FRAP) activity of nanoliposomes loaded with the optimized microalgal extract (Dt-LN) and β-carotene (β-CAR-LN). The FRAP assay specifically measures the electron-donating capacity of the released bioactive compounds by assessing their ability to reduce $Fe^{3+}$ (ferric ion) to $Fe^{2+}$ (ferrous ion), reflecting their potential as reducing agents and antioxidants.

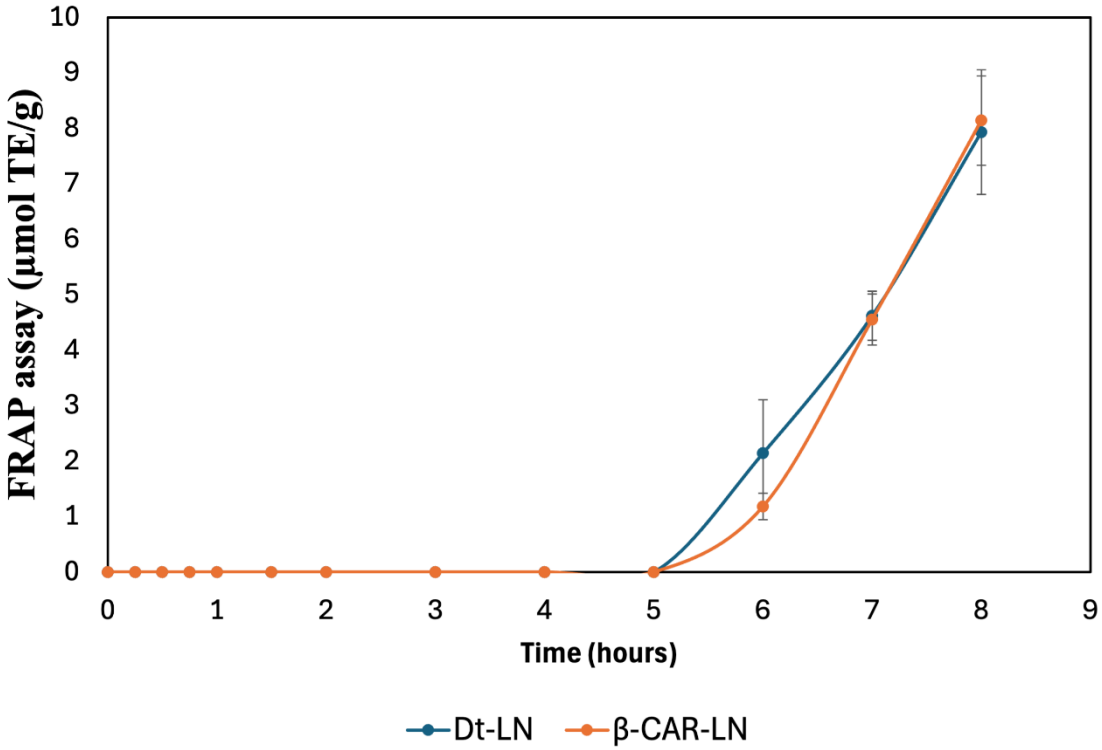


**Figure 11.** Sustained-release kinetics of the nano-liposomes loaded with microalgal extract and β-carotene on FRAP.

The release kinetics observed in this assay clearly demonstrate a prolonged and controlled release behavior for both nanoformulations, with the antioxidant activity initiating after a lag phase and progressively increasing over time, reaching its maximum after 8 hours. This gradual increase indicates that the encapsulated bioactive compounds are not released immediately but rather follow a controlled release mechanism, governed by the diffusion of the compounds through the nanoliposomal bilayer and their interaction with the lipid matrix.

The kinetic profiles of both Dt-LN and β-CAR-LN formulations show negligible ferric reducing activity during the initial 5 hours of incubation, suggesting effective retention of the active compounds within the nanoliposomal system and minimal early leakage. This delayed onset is characteristic of sustained-release systems, where the encapsulated compounds diffuse slowly from the lipid core to the external medium, likely following a Fickian diffusion-controlled mechanism. The subsequent sharp increase in FRAP values after 5 hours reflects the progressive release and

 doi:10.20944/preprints202508.0483.v1



accumulation of the bioactive molecules into the medium, where they become available to participate in the electron transfer reactions required for $Fe^{3+}$ reduction [59,60].

At the molecular level, the FRAP assay operates through a single electron transfer (SET) mechanism, wherein antioxidants act as electron donors to reduce the ferric-tripyridyltriazine ($Fe^{3+}$-TPTZ) complex to its ferrous form ($Fe^{2+}$-TPTZ), which is quantified spectrophotometrically. The observed antioxidant activity, therefore, directly correlates with the presence and release rate of effective electron-donating molecules from the nanoliposomal systems. In this context, carotenoids, chlorophyll derivatives, and other antioxidant metabolites present in the microalgal extract or β-carotene are responsible for donating electrons via SET to drive the reduction process. The slow, sustained increase in FRAP activity indicates that the integrity of the nanoliposome structure effectively modulates the release, preventing the immediate availability of these reducing agents and promoting a gradual delivery instead [61].

Interestingly, although both formulations exhibited similar release patterns, the Dt-LN system showed a slightly earlier onset of FRAP activity compared to β-CAR-LN, which could be attributed to the complex composition of the microalgal extract, containing both hydrophilic and lipophilic compounds with varying affinities to the lipid bilayer. This heterogeneous mixture may facilitate a broader range of interactions with the lipid matrix, resulting in a more gradual but sustained release of the electron-donating molecules. In contrast, the β-carotene-loaded liposomes, containing a single hydrophobic molecule, may exhibit a slower diffusion process through the liposomal membrane due to the strong interaction between β-carotene and the hydrophobic lipid core.

These findings confirm that nanoliposomal encapsulation of microalgal extract and β-carotene enables controlled, sustained antioxidant release with prolonged bioactivity. The FRAP assay (SET mechanism) highlights functional release performance, supporting their potential in nutraceutical, food, or biomedical applications. This sustained-release behavior may improve oxidative balance, reduce dosing frequency, and enhance bioactive compound stability and bioavailability. The sustained-release behavior and antioxidant activity of Dt-LN and β-CAR-LN, assessed via ABTS and FRAP assays, revealed a controlled, prolonged release of encapsulated bioactives. The ABTS assay, sensitive to both hydrogen atom transfer (HAT) and single electron transfer (SET) mechanisms, showed early and continuous antioxidant activity over 8 hours, indicating effective release of both surface-bound and encapsulated compounds. In contrast, the FRAP assay, which detects only SET-based activity, displayed a delayed response with a clear lag phase in the first 5 hours, followed by a marked increase in reducing power. This suggests that ABTS captures early scavenging by a broader range of antioxidants, while FRAP reflects the gradual release and accumulation of stronger electron-donating compounds. Together, these assays confirm the nanoliposomes' ability to provide sustained and phase-dependent antioxidant release, offering complementary insights into the release kinetics and mechanisms of action of the encapsulated compounds [2–4].

### *2.9. Antioxidant Activity of Nanoliposomal Formulations*

The data presented in Table 4 show the antioxidant activity of different treatments, including nanoliposomes loaded with *Dunaliella tertiolecta* extract (Dt-NL), β-carotene-loaded nanoliposomes (β-CAR-NL), unloaded nanoliposomes (NC-NL), free microalgal extract, and commercial β-carotene, evaluated through $ABTS^{\bullet+}$ radical scavenging and ferric reducing antioxidant power (FRAP) assays. The results indicate that all loaded formulations exhibited significantly higher antioxidant activity compared to the unloaded control (NC-NL), which showed no detectable activity in either assay. Among the samples, the microalgal extract and commercial β-carotene in free form demonstrated the highest antioxidant capacities, particularly in the FRAP assay, with values of 47.62 ± 0.88 μmol TE/g and 49.45 ± 0.6 μmol TE/g, respectively. These high FRAP values suggest a potent electron-donating capacity, characteristic of both chlorophyll derivatives and carotenoids present in the microalgal extract, as well as the β-carotene molecule itself.

 doi:10.20944/preprints202508.0483.v1



**Table 4.** Antioxidant activity assessed by ABTS$^{\bullet+}$ and FRAP assays for nanoliposomes loaded with *Dunaliella tertiolecta* extract, β-carotene, unloaded nanoliposomes, microalgal extract, and commercial β-carotene.

| Sample | ABTS$^{\bullet+}$ (µmol TE/g) | FRAP (µmol TE/g) |
|---|---|---|
| ***Dt*-NL** | 12.44 ± 0.12$^{c}$ | 46.11 ± 0.83$^{c}$ |
| **β-CAR-NL** | 10.8 ± 0.17$^{b}$ | 41.52 ± 1.14$^{b}$ |
| **NC-NL** | 0$^{a}$ | 0$^{a}$ |
| **Microalgal extract** | 12.92 ± 0.11$^{d}$ | 47.62 ± 0.88$^{cd}$ |
| **β-Carotene** | 12.41 ± 0.16$^{c}$ | 49.45 ± 0.6$^{d}$ |

Different letters within the same column indicate significant differences between treatments at $p < 0.05$.

Interestingly, the Dt-NL formulation exhibited antioxidant activities of 12.44 ± 0.12 µmol TE/g (ABTS•$^{+}$) and 46.11 ± 0.83 µmol TE/g (FRAP), comparable to the free microalgal extract, particularly in the FRAP assay where no statistically significant differences were observed between Dt-NL and the microalgal extract. In contrast, β-CAR-NL showed slightly lower antioxidant capacity (10.8 ± 0.17 µmol TE/g in ABTS•$^{+}$ and 41.52 ± 1.14 µmol TE/g in FRAP) than Dt-NL, supporting the idea that the presence of a complex mixture of bioactive compounds in the microalgal extract may offer synergistic effects that enhance antioxidant potential beyond what β-carotene alone can achieve. The superior performance of the microalgal extract and Dt-NL in the FRAP assay, which operates exclusively through a single electron transfer (SET) mechanism, suggests a strong capacity for reducing ferric ions, while the ABTS•$^{+}$ assay, sensitive to both SET and hydrogen atom transfer (HAT) mechanisms, revealed moderate but effective radical scavenging activity.

From a bioavailability and functionality standpoint, nanoliposomal encapsulation offers key advantages for protecting sensitive antioxidant compounds like carotenoids and pigments during gastrointestinal transit. The lipid bilayer serves as a barrier against harsh digestive conditions, preserving the structural integrity and antioxidant activity of the encapsulated molecules until their controlled release in the intestine. The amphiphilic nature of nanoliposomes also enhances the solubility and absorption of hydrophobic compounds such as β-carotene, improving bioavailability. Results indicate that Dt-NL maintains comparable antioxidant activity to the free microalgal extract, with the added benefit of sustained protection and gradual release. While the free forms showed slightly higher immediate activity, encapsulation ensures prolonged efficacy during digestion, crucial for functional and nutraceutical applications. This improved performance is attributed to the chemical structure of carotenoids, whose conjugated double bonds and terminal rings enable electron donation and resonance stabilization, preserving their antioxidant activity [55].

### *2.10. Erythroprotective Potential of Loaded Nano-Liposomes*

The results presented in the Table 5 demonstrate that nanoliposomes loaded with Dunaliella tertiolecta extract (Dt-LN) and β-carotene-loaded nanoliposomes (β-CAR-LN) exhibited significantly higher erythroprotective effects compared to unloaded nanoliposomes (UL-N), which showed minimal hemolysis inhibition across all analyzed blood groups (A+, B-, O+, AB+). This finding indicates that the protective effect is directly associated with the presence of bioactive compounds incorporated within the nanoliposomes rather than the liposomal structure itself. Among the evaluated treatments, free β-carotene displayed the highest percentage of hemolysis inhibition, reaching up to 94.70 ± 3.83% in the A+ group and 94.66 ± 3.86% in the O+ group, highlighting its strong antioxidant efficacy in neutralizing free radicals and preserving erythrocyte membrane integrity. However, the microalgal extract also exhibited a considerable antioxidant potential, though lower than that of pure β-carotene, possibly due to the synergistic action of multiple antioxidant compounds present in the algal biomass contributing to hemolysis inhibition.

 doi:10.20944/preprints202508.0483.v1



**Table 5.** Erythroprotective potential of nanoliposomes loaded with *Dunaliella tertiolecta* extract and β-carotene against oxidative damage on human erythrocytes.

| | Hemolysis inhibition (%) | | | |
|---|---|---|---|---|
| **Sample** | **A⁺** | **B⁻** | **O⁺** | **AB⁺** |
| ***Dt*-LN** | 53.17 ± 4.66$^{b}$ | 49.67 ± 3.79$^{b}$ | 54.84 ± 8.82$^{b}$ | 45.53 ± 7.6$^{c}$ |
| **β-CAR- LN** | 50.04 ± 10.42$^{b}$ | 47.11 ± 6.17$^{b}$ | 49.63 ± 10.5$^{b}$ | 39.03 ± 6.5$^{bc}$ |
| **UL-N** | 8.72 ± 0.42$^{a}$ | 8.54 ± 0.34$^{a}$ | 8.4 ± 0.4$^{a}$ | 8.56 ± 0.33$^{a}$ |
| **Microalgal extract** | 46.62 ± 4.66$^{b}$ | 51.22 ± 2.06$^{b}$ | 46.45 ± 4.6$^{b}$ | 28.12 ± 4.62$^{b}$ |
| **β-carotene** | 94.70 ± 3.83$^{c}$ | 75.55 ± 10.89$^{c}$ | 94.66 ± 3.86$^{c}$ | 47.69 ± 1.67$^{c}$ |

Different letters within the same column indicate significant differences between treatments at $p < 0.05$. Dt-LN= *Dunaliella tertiolecta*-Loaded Nanoliposome; β-Car-LN= β-Carotene-Loaded Nanoliposome; UL-N= unloaded nanoliposomes.

The mechanism underlying these results involves the inhibition of hemolysis induced by AAPH, a compound that generates peroxyl radicals through thermal decomposition, triggering lipid peroxidation in erythrocyte membranes and leading to hemoglobin (Hb) release. Measuring released Hb by spectrophotometry serves as an indirect indicator of oxidative damage, where lower Hb levels indicate stronger anti-hemolytic (erythroprotective) activity. Nanoliposomes enhance the stability and controlled release of encapsulated antioxidants, improving their interaction with AAPH-generated radicals and extending their protective effect. This explains the superior performance of encapsulated versus free compounds, confirming nanoliposomes as effective delivery systems for prolonging antioxidant action and protecting red blood cells from oxidative stress [57,58].

Moreover, it is important to emphasize that the encapsulation of β-carotene and *D. tertiolecta* extract within nanoliposomes allows for sustained release and potentially higher bioavailability at the site of oxidative stress generation, providing continuous protection against radical-induced membrane damage. The differential efficacy between free and encapsulated antioxidants may also be attributed to the release kinetics and the interaction dynamics of the bioactive compounds with the erythrocyte membrane surface, where nanoliposomes facilitate close contact with the cellular targets. This protective strategy reinforces the relevance of designing sustained-release delivery systems to prevent oxidative damage, particularly in sensitive cellular models such as erythrocytes [58].

Regarding the variability observed among different blood groups, it is important to consider that erythrocyte membrane composition differs between A+, B-, O+, and AB+ groups due to the presence of specific surface antigens (agglutinogens), which may influence susceptibility to oxidative damage and the interaction with antioxidant compounds. These structural differences can affect the arrangement of membrane glycoproteins and sphingolipids, modifying the accessibility of free radicals to vulnerable lipid sites. Therefore, evaluating the antioxidant effect and erythroprotective potential across different blood groups provides valuable insight into potential variations in therapeutic response, supporting the development of personalized antioxidant strategies. This approach could be particularly relevant in preventing oxidative stress-related complications in hematological and cardiovascular disorders, considering individual blood group characteristics to optimize nutraceutical formulations and clinical applications [1,3].

### *2.5. Citotoxicity of Loaded Nano-Liposomes*

The cytotoxicity results presented in the Table 6 reveal notable differences in the percentage of hemolysis induced by the various treatments across the different erythrocyte blood groups. Both nanoliposomes loaded with *Dunaliella tertiolecta* extract (Dt-LN) and β-carotene-loaded nanoliposomes (β-CAR-LN) exhibited moderate cytotoxicity values, generally higher than those

 doi:10.20944/preprints202508.0483.v1



observed for unloaded nanoliposomes (UL-N), particularly in blood types A+, B-, and O+. This suggests that while the incorporation of bioactive compounds into nanoliposomal systems enhances their erythroprotective potential, it may also slightly increase membrane interaction, potentially leading to higher hemolytic activity under oxidative conditions. Notably, free β-carotene consistently demonstrated the lowest cytotoxicity values among the treatments in most blood groups, with percentages as low as 2.36 ± 0.85% in A+ and 5.7 ± 0.69% in AB+, highlighting its biocompatibility and safe profile for erythrocyte membranes.

**Table 6.** Citotoxicity (%) for nanoliposomes loaded with *Dunaliella tertiolecta* extract and β-carotene against oxidative damage on human erythrocytes.

| | Citotoxicity (%) | | | |
|---|---|---|---|---|
| **Sample** | **A⁺** | **B⁻** | **O⁺** | **AB⁺** |
| ***Dt*-LN** | 17.22 ± 3.31$^{c}$ | 20.46 ± 4.39$^{b}$ | 21.62 ± 4.52$^{b}$ | 6.59 ± 1.01$^{a}$ |
| **β-CAR- LN** | 17.48 ± 3.07$^{c}$ | 14.94 ± 1.56$^{a}$ | 15.92 ± 1.61$^{a}$ | 22.25 ± 3.76$^{d}$ |
| **UL-N** | 11.22 ± 2.21$^{b}$ | 12.34 ± 2.25$^{a}$ | 13.24 ± 2.04$^{a}$ | 10.57 ± 1.47$^{b}$ |
| **Microalgal extract** | 20.47 ± 1.79$^{c}$ | 22.47 ± 1.98$^{b}$ | 23.68 ± 2.04$^{b}$ | 15.33 ± 1.87$^{c}$ |
| **β-carotene** | 2.36 ± 0.85$^{a}$ | 13.88 ± 1.91$^{a}$ | 14.83 ± 1.95$^{a}$ | 5.7 ± 0.69$^{a}$ |

Different letters within the same column indicate significant differences between treatments at $p < 0.05$. Dt-LN= *Dunaliella tertiolecta*-Loaded Nanoliposome; β-Car-LN= β-Carotene-Loaded Nanoliposome; UL-N= unloaded nanoliposomes.

The mechanism underlying these cytotoxicity results is closely linked to oxidative stress-induced hemolysis caused by bioactive compounds. Radical generation attacks the phospholipid bilayer of erythrocyte membranes, promoting lipid peroxidation and structural destabilization, leading to hemoglobin (Hb) release into the extracellular medium. The amount of Hb released, measured spectrophotometrically, indicates the extent of membrane damage, with higher Hb levels reflecting greater oxidative damage and cytotoxicity. While nanoliposome delivery systems enhance the efficacy of antioxidant agents, they may also increase interaction with erythrocyte membranes, potentially elevating oxidative damage depending on the concentration and release rate of encapsulated compounds. Interestingly, the microalgal extract showed cytotoxicity levels comparable to or slightly higher than nanoliposome-encapsulated treatments, especially in B- and O+ blood groups, likely due to other active metabolites in the extract interacting with cell membranes. Variations between free and encapsulated β-carotene highlight how nanoencapsulation modulates bioactivity and membrane interaction, reinforcing the need to optimize nanocarrier systems to balance antioxidant benefits with minimal cytotoxic effects [23,50].

The variability in cytotoxic responses observed among the different erythrocyte blood groups can be explained by the distinct composition and structural organization of membrane surface antigens (agglutinogens) present in each blood type (A+, B-, O+, AB+). These antigens, composed primarily of glycoproteins and glycolipids, influence the biophysical properties of the erythrocyte membrane, including fluidity, charge distribution, and susceptibility to oxidative damage. Such differences may modulate the interaction of bioactive compounds and nanoliposomes with the membrane, leading to varying degrees of hemolytic response. Studying these variations across blood groups is essential for the development of targeted antioxidant therapies and the design of biocompatible delivery systems tailored to individual patient profiles. This approach could have significant clinical applications in personalized medicine, particularly in preventing oxidative damage in transfusion medicine, anemia management, and cardiovascular health, where erythrocyte stability plays a critical role [1,23].

 doi:10.20944/preprints202508.0483.v1



*2.11. Scanning Electron Microscopy (SEM)*

Nano-liposomes prepared via particle dispersion method were observed under a scanning electron microscope to characterize the morphology and shape. Samples were observed in a range of 500x to 5000x magnification to confirm the ocurrence of well formed nano-sized and spherical liposomes. Figure 5 is divided into 4 images, two corresponding to Dt-NL and two to β-CAR-NL. Figure 12 shows scanning electron microscopy (SEM) micrographs of nanoliposomes loaded with the microalgal extract (Figures A and B) and β-carotene (Figures C and D), providing detailed insights into the morphology and surface characteristics of the nanoliposomal systems. The images at different magnifications clearly illustrate distinct structural features between the two types of loaded nanoliposomes, which are critical for understanding their release behavior, stability, and functional properties.

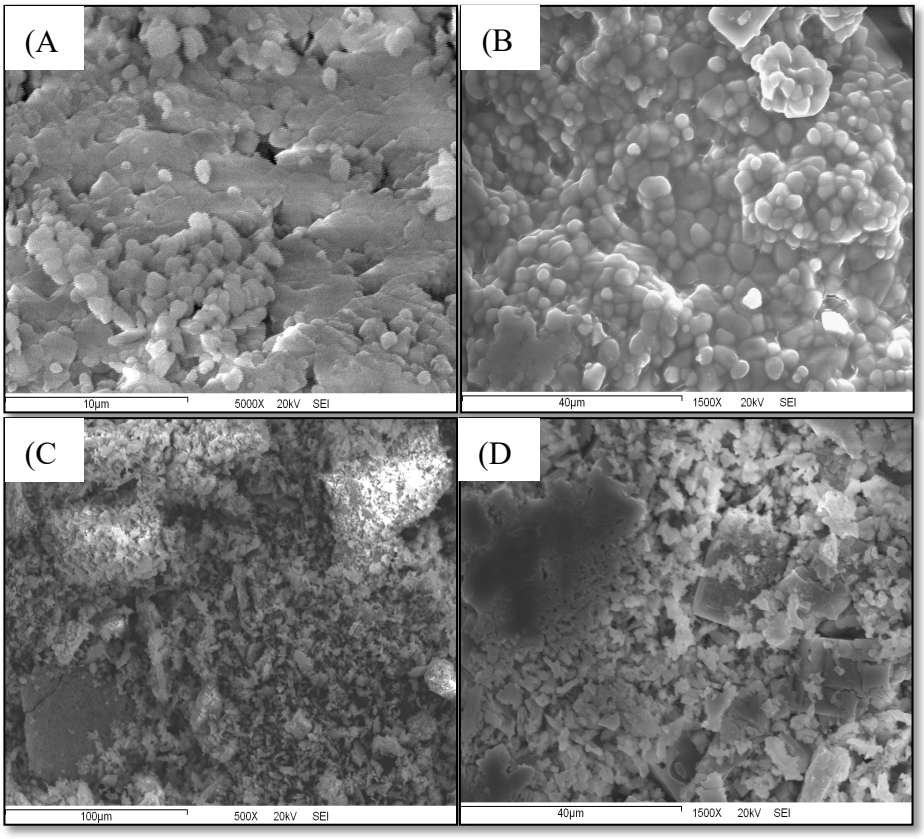


**Figure 12.** SEM micrographs of nano-liposomes loaded with microalgal extract (A and B) and β-carotene (C and D).

In the micrographs of the Dt-LN formulation (Figures 12A and 12B), nanoliposomes display a uniform spherical to semi-spherical morphology with a dense, compact surface and strong aggregation, suggesting close interaction among lipid vesicles. At higher magnification (5000×), the smoother surface indicates effective encapsulation of the microalgal extract, likely contributing to reduced permeability and a slower diffusion rate of bioactives. These features align with the sustained release observed in antioxidant assays, as the compact structure may act as a barrier to rapid release. In contrast, SEM images of β-CAR-LN (Figures 12C and 12D) show a more irregular, porous morphology with rough surfaces, visible cracks, and loosely aggregated particles. This less compact structure likely results from interactions between hydrophobic β-carotene and the lipid bilayer, leading to less stable vesicle formation. Consequently, the β-CAR-LN formulation may allow faster release of encapsulated compounds, particularly under digestive conditions where bile salts and enzymes disrupt nanocarrier integrity [16,22].

 doi:10.20944/preprints202508.0483.v1



From a functional perspective, these morphological characteristics have direct implications on the release kinetics, stability, and antioxidant functionality of the nanoliposomal formulations. The denser and smoother surface of Dt-LN suggests enhanced physical stability by limiting oxidative degradation and premature release of the encapsulated compounds, promoting a prolonged and controlled release profile as confirmed by the ABTS and FRAP assays. This structural integrity is essential for protecting sensitive bioactives like chlorophylls and carotenoids throughout processing, storage, and gastrointestinal transit. On the other hand, the β-CAR-LN system, with its more porous and less cohesive morphology, may exhibit faster release kinetics due to the easier penetration of aqueous media into the vesicle core and potential structural collapse under physiological conditions. While this may lead to higher initial bioavailability, it could also compromise long-term stability and result in faster degradation of β-carotene, which is highly susceptible to oxidation when exposed to environmental factors [22].

SEM analysis confirms that morphological differences between Dt-LN and β-CAR-LN nanoliposomes significantly influence their release behavior, stability, and antioxidant performance. The compact, uniform structure of Dt-LN supports prolonged delivery and sustained antioxidant activity, making it more suitable for functional food and nutraceutical applications. In contrast, the β-CAR-LN formulation, with its porous, irregular morphology, may require optimization to improve structural integrity and control release. Size analysis revealed that Dt-LN nanoliposomes ranged mostly between 200–500 nm with consistent, compact morphology, while β-CAR-LN showed greater heterogeneity, with some vesicles reaching 600 nm and forming irregular aggregates. This smaller, more homogeneous size distribution in Dt-LN aligns with enhanced stability and a sustained-release profile. Conversely, the larger, less cohesive β-CAR-LN structures may facilitate faster diffusion but could compromise long-term stability and protection of the encapsulated bioactives. These findings underscore the importance of morphological characterization in designing effective nanocarrier systems [16,22].

### *2.12. Fourier Transform Infrared Spectroscopy (FT-IR)*

The Fourier-transform infrared (FT-IR) spectra presented in Figure 13 provide a comparative analysis of the functional group composition across unloaded nanoliposomes (NC-LN), nanoliposomes loaded with Dunaliella tertiolecta extract (Dt- LN), β-carotene-loaded nanoliposomes (β-CAR- LN), the microalgal extract, and commercial β-carotene. In the β-carotene spectrum (11E), characteristic vibrational bands are clearly observed around 3020–3000 $cm^{-1}$ (C–H stretching of aromatic rings) and near 1600 $cm^{-1}$ (C=C stretching of conjugated polyene chains), confirming the presence of its highly conjugated hydrocarbon backbone. Similar bands appear in the microalgal extract (11D), supporting the presence of carotenoids such as β-carotene and xanthophylls (e.g., lutein, violaxanthin). Additional broad O–H stretching bands around 3650–3300 $cm^{-1}$ in the microalgal extract suggest the coexistence of hydroxylated carotenoids (xanthophylls), possibly along with other polar compounds like chlorophyll derivatives or phenolics, not present in the pure β-carotene spectrum.

 doi:10.20944/preprints202508.0483.v1



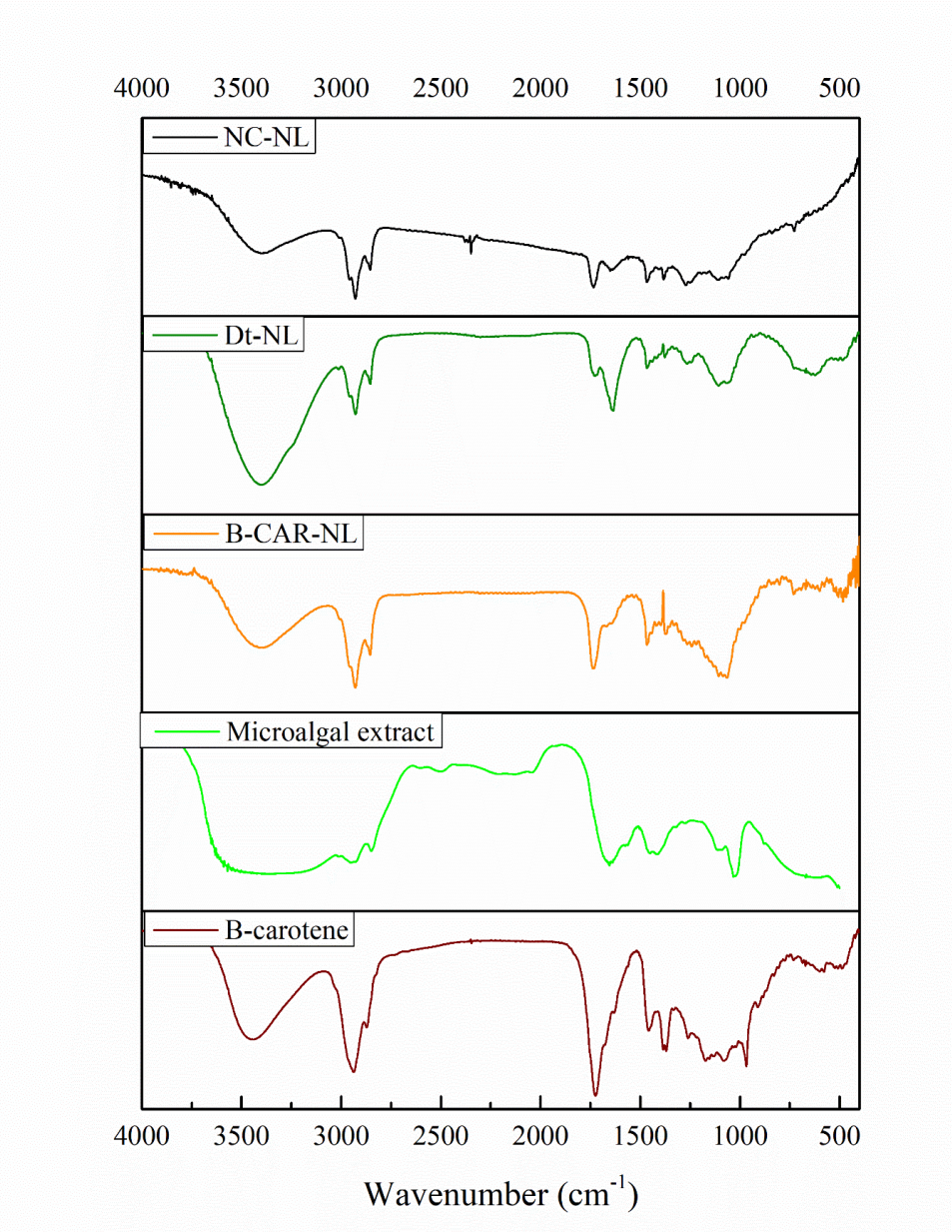


**Figure 13.** Fourier transform infrared (FT-IR) spectra of NC-NL (unloaded nanoliposomes), Dt-NL (nanoliposomes loaded with Dunaliella tertiolecta extract), β-CAR-NL (β-carotene-loaded nanoliposomes), microalgal extract and commercial β-carotene.

In the Dt-NL spectrum, the presence of these characteristic carotenoid bands is preserved, confirming successful encapsulation of pigments into the lipid matrix. The O–H stretching band is broadened, and additional signals in the region between 1700 and 1735 $cm^{-1}$ (C=O stretching) appear, likely due to ester linkages from the phospholipid bilayers of the nanoliposomes interacting with the encapsulated compounds. This feature is shared with the NC-NL and β-CAR-NL spectra, indicating the structural contribution of the phospholipid components. However, Dt-NL and β-CAR-NL display a more complex spectral pattern compared to NC-NL, confirming the successful incorporation of bioactive molecules within the vesicles. Notably, β-CAR-NL exhibits weaker O–H signals, consistent with the non-polar nature of β-carotene, and shows C=O stretching signals due to the liposomal structure rather than from the carotenoid itself [18,27].

Structurally and molecularly, the preservation of the carotenoid-related signals, particularly the conjugated C=C stretching (~1600 $cm^{-1}$) and aromatic C–H (~3020–3000 $cm^{-1}$) bands, alongside lipid-associated ester (C=O) peaks, supports the integrity of the encapsulated β-carotene and microalgal carotenoids within the nanoliposomal systems. The broader O–H signals in Dt-NL and the microalgal

 doi:10.20944/preprints202508.0483.v1



extract reflect the complex nature of these matrices, which may include xanthophylls and other polar metabolites that could influence the antioxidant capacity and release behavior of the formulations. The FT-IR data validate the encapsulation process, confirm the presence of key functional groups associated with carotenoids, and suggest potential molecular interactions between the encapsulated pigments and the lipid bilayer, which may contribute to the controlled release and stability observed in the antioxidant assays [27,58].

FT-IR spectroscopy is a key tool for characterizing nanoliposomal systems, offering insights into functional groups and molecular interactions between encapsulated bioactives and the lipid matrix. It confirms successful encapsulation by identifying characteristic vibrational bands of both the active compounds and phospholipid bilayers, providing evidence of chemical stability and potential bonding. In this study, FT-IR verified the incorporation of carotenoids, including β-carotene and pigments from Dunaliella tertiolecta, by detecting bands associated with conjugated double bonds (C=C), aromatic C–H stretching, and ester carbonyl groups (C=O). Spectral differences between unloaded and loaded nanoliposomes suggested interactions with the lipid bilayer, relevant to encapsulation efficiency, stability, and release behavior. This structural validation supports the integrity and functionality of the nanoliposomes, enhancing understanding of their performance in antioxidant delivery applications [18].

The FT-IR analysis presented in Table 7 provides a detailed identification of the functional groups present in the loaded nanoliposomes (Dt-NL, β-CAR-NL, NC-NL), the microalgal extract of Dunaliella tertiolecta, and commercial β-carotene. The presence of characteristic vibrational bands in the range of ~3020–3000 $cm^{-1}$ (C–H stretching of aromatic rings) and ~1600 $cm^{-1}$ (C=C stretching) confirms the existence of conjugated double bond systems, which are typical of carotenoids. In particular, the identification of these bands in both the Dt-NL formulation and the microalgal extract suggests the presence of carotenoid pigments with polyene chains, including β-carotene, lutein, and violaxanthin, all of which are commonly synthesized by D. tertiolecta. The detection of O–H stretching bands (~3650–3300 $cm^{-1}$) across all samples corresponds to alcohol functional groups, likely related to hydroxylated carotenoids (xanthophylls) such as lutein or zeaxanthin, and to possible residual water content or hydroxyl groups from the phospholipid bilayers of the nanoliposomes. Additionally, the presence of C=O stretching signals between 1730–1700 $cm^{-1}$, particularly in NC-NL and Dt-NL, can be associated with ester groups from phospholipid molecules or esterified carotenoids [18,59].

**Table 7.** Functional groups identified in the loaded nanoliposomes, microalgal extract, and β-carotene using Fourier-transform infrared spectroscopy (FT-IR).

| Functional group | Band | Wavenumber ($cm^{-1}$) | Present in |
|---|---|---|---|
| **Alkynes** | C-H (acetylenic) | ~3300 | Microalgal extract |
| **Aromatic** | C-H | ~3020-3000 | All |
| | C=C | ~1600 | *Dt*-NL and microalgal extract |
| **Alcohols** | O-H | ~3650-3300 | All |
| **Carboxylic acids** | O-H | 3400-2400 | *Dt*-NL and microalgal extract |
| | C=O | 1730-1700 | NC-NL and *Dt*-NL |
| **Amines** | N-H | 3500-3180 | *Dt*-NL and microalgal extract |
| | C-N | ~1200 | *Dt*-NL and microalgal extract |

 doi:10.20944/preprints202508.0483.v1



| | | | |
|---|---|---|---|
| **Amides** | N-H | ~1640 | *Dt*-NL and microalgal extract |
| **Alkanes** | C-H | 2950-2800 | All |
| | $C\text{-}H_2$ | ~1450 | All |
| **Alkenes** | C=C (Isolated) | ~1690 | All |
| | C=C (Conjugated) | ~1640 | *Dt*-NL and microalgal extract |
| | C-H | ~1430 | All |
| **Esters** | C=O | 1750-1735 | NC-NL, β-CAR-NL and β-carotene |
| **Nitro groups** | $-NO_2$ (aliphatic) | ~1390 | *Dt*-NL and microalgal extract |

Structurally, the identification of N–H stretching (3500–3180 $cm^{-1}$), C–N (~1200 $cm^{-1}$), and amide N–H bending (~1640 $cm^{-1}$) bands in Dt-NL and the microalgal extract suggests interactions between amino acid residues or protein-like components and the encapsulated pigments, supporting the notion of a complex extract composition. The detection of alkene C=C conjugated systems (~1640 $cm^{-1}$) further confirms the predominance of polyunsaturated carotenoids with extensive π-electron delocalization, which is a hallmark of β-carotene and related compounds. Importantly, the alkane C–H (~2950–2800 $cm^{-1}$) and $C\text{–}H_2$ (~1450 $cm^{-1}$) stretching bands observed across all samples reflect the lipidic nature of the nanocarriers. The presence of esters (C=O 1750–1735 $cm^{-1}$) specifically in NC-NL, β-CAR-NL, and commercial β-carotene also aligns with the molecular structure of β-carotene derivatives and the phospholipid matrix. Moreover, the identification of alkyne C–H stretching (~3300 $cm^{-1}$) and nitro groups ($-NO_2$ at ~1390 $cm^{-1}$) in the microalgal extract and Dt-NL may indicate additional complex metabolites, including oxidized or nitrogen-containing carotenoid derivatives. Overall, the FT-IR results confirm the presence of β-carotene in the D. tertiolecta extract, alongside other xanthophylls, through the characteristic polyene and aromatic signals, supporting the structural diversity of the pigment profile and validating the successful encapsulation of these bioactives within the nanoliposomal systems [18,27].

## 3. Materials and Methods

### *3.1. Chemical Reagents*

The chemical reagents employed throughout this research included food-grade β-carotene, soy phosphatidylcholine (SPC), cholesterol, DPPH (1,1-diphenyl-2-picrylhydrazyl), ABTS [2,2′-azinobis (3-ethylbenzothiazoline)-6-sulfonic acid), dimethyl sulfoxide (DMSO), sodium acetate buffer, ferric chloride ($FeCl_3$), TPTZ (2,4,6-tripyridyl-s-triazine), Triton X-100, AAPH [2,2′-azobis (2-methylpropionamidine) dihydrochloride], and phosphate-buffered saline (PBS). All reagents were procured from Sigma-Aldrich Co. (St. Louis, MO, USA). Additionally, the solvents used for the different analytical procedures were of analytical grade and ensured to be of the highest commercially available purity.

### *3.2. Biological Material and Ethical Considerations*

All experimental procedures involving human red blood cells (RBCs) were performed following international ethical standards and regulations, including the FDA guidelines (CFR—Code of Federal Regulations Title 21, Part 640, Subpart B: Red Blood Cells, Section 640.14 Blood Tests [21 CFR 640.14]), as well as the Official Mexican Standard NOM-253-SSA1-2012 [62], which specifies the requirements for the collection, processing, and therapeutic use of human blood and its components. The erythrocyte membranes utilized in this study were obtained from the clinical analysis laboratory at

 doi:10.20944/preprints202508.0483.v1



the University of Guadalajara, a facility accredited under ISO-IEC 17025 (NMX-EC-17025) and ISO 15189 standards, developed by the ISO/TC 212 technical committee on clinical laboratory testing and in vitro diagnostic systems. These accreditations, along with ISO/IEC 17025 and ISO 9001, ensure the quality and reliability of the procedures followed [63–65].

Blood samples were collected from healthy adult volunteers aged between 20 and 40 years, with an erythrocyte concentration ranging from approximately 4.7 to 6.1 × $10^6$ cells/µL. Prior to blood collection, all participants provided written informed consent. Venous blood sampling was performed using sterile techniques, with EDTA employed as an anticoagulant to preserve the red blood cells. The use of erythrocyte membranes in this research served as a cellular model to assess the erythroprotective properties of the yogurt formulation under study **[66,67]**. The research protocol was reviewed and approved by the corresponding institutional ethics committee (Approval Code: CI 2023-47).

### *3.3. Microalgae Strain and Growth Kinetics of Dunaliella tertiolecta*

The marine microalgae Dunaliella tertiolecta was obtained from the strain collection of the "Department of Scientific and Technological Research, University of Sonora (DICTUS)". The bioassays were conducted in 1 L Erlenmeyer flasks containing 700 mL of culture medium, under controlled conditions of temperature (20 ± 1 °C) and light intensity (274 ± 52.5 µmol photons $m^{-2}$ $s^{-1}$). The cultures were maintained using the F/2 medium, as described by Guillard and Ryther (1962), which contains nitrates, phosphates, silicates, trace metals, and vitamins.

Table 8 summarizes the different culture media employed to evaluate the microalgae's growth behavior and adaptation under various cellular stress conditions, including nitrogen deprivation and varying salinity levels. The standard F/2 medium, prepared with 0.88 mol·$L^{-1}$ sodium nitrate ($NaNO_3$) at 35 practical salinity units (PSU), is widely recognized as the optimal medium for microalgae cultivation in aquaculture research. It is important to note that these experimental treatments were exclusively applied for the assessment of growth kinetics.

**Table 8.** Completely random factorial design of the treatments (nitrogen concentration and different salinities) applied in the microalgae culture.

| Nitrogen concentration | Salinity (PSU) |
|---|---|
| 0.88 mol·$L^{-1}$ (1)* | 25 |
| | 35 |
| | 45 |
| 0.44 mol·$L^{-1}$ (0.5)* | 25 |
| | 35 |
| | 45 |
| 0.22 mol·$L^{-1}$ (0.25)* | 25 |
| | 35 |
| | 45 |

* mL de $NaNO_3$ for each litter of seawater for culture.

The growth kinetics of Dunaliella tertiolecta were evaluated under culture conditions using the optimized medium specifically designed to enhance both microalgal growth and the production of antioxidant pigments. The microalgae cultures were monitored over a period of 21 days, covering all growth phases. To determine the growth kinetics, 1 mL of culture from each treatment was collected daily. Lugol's solution ($I_2$ 1% and KI 2% in distilled water) was added to each sample to fix the cells and facilitate counting. The fixed samples were then loaded into a Neubauer hemocytometer (0.1 mm depth). Cell enumeration was performed using a compound optical microscope (Olympus CX43,

 doi:10.20944/preprints202508.0483.v1



Olympus Europe). Cell density was calculated according to Equation 7, following the methodology described by Goiris [5].

$$Eq.7: \left(\#\frac{Cells}{8}\right) * 10{,}000 = \frac{\#Cells}{mL} \quad (7)$$

*3.4. Experimental Design and Statistical Optimization for Pigment Production*

To optimize pigment production, a central composite design (CCD) was employed, with a minimum of three replicates per treatment (n ≥ 3). The interactions between the independent variables at different levels were systematically evaluated. The independent variables included low-nitrogen concentration media (0.22 and 0.88 mol·L$^{-1}$), varying salinity levels (25, 35, and 45 PSU), and culture age (harvest day). The CCD was structured based on a second-order polynomial model (Equation (8)):

$$Eq\ 8: Y = \beta_0 \sum_{i=1}^{k} \beta_i X_i + \sum_{i=1}^{k} \beta_{ii} X_{ii}^2 + \sum_{i}^{k-1} \sum_{j}^{k} \beta_{ij} X_i X_j + \varepsilon \quad (8)$$

where Y represents the response variable, $\beta_0$ is the intercept, $\beta_{ki}$ denotes the linear regression coefficients, $\beta_{kii}$ represents the quadratic regression coefficients, $\beta_{kji}$ corresponds to the interaction coefficients between variables, and ε is the experimental error term. Culture conditions were optimized to maximize pigment production and enable accurate quantification. The responses analyzed using Equation (8) included chlorophyll a, chlorophyll b, chlorophyll c, total chlorophyll, total carotenoids, and overall pigment yield.

The optimization matrix was constructed with an integrated ANOVA (analysis of variance) using JMP V18, considering statistical significance at $p < 0.05$. Following matrix generation, a lack-of-fit test ($p > 0.05$) was performed to confirm the adequacy of the model and to ensure that the predicted values appropriately fit the experimental data. The relationship between the independent variables and the responses was modeled using Equation (2). The total number of experimental runs (N) required for the CCD was determined using the equation: N = 2^k (k – 1) + $C_0$,, where k represents the number of factors and $C_0$ denotes the number of replicates at the central point of the design. CCD was specifically chosen due to its efficiency in reducing the number of experimental runs required when three variables are involved. Based on the variance analysis, regression coefficients for linear, quadratic, and interaction terms were calculated [24].

*3.5. Response Surface Methodology (RSM)*

Response Surface Methodology (RSM) was applied to evaluate the influence of nitrogen concentration (NC), salinity, and culture age (AC) on six response variables: chlorophyll a, chlorophyll b, chlorophyll c, total chlorophyll, total carotenoids, and overall pigment yield. Overlay plots were used as part of the optimization technique to generate response surface graphics. To visualize the relationships between the experimental factors and the responses, regression coefficients derived from the fitted polynomial equation were used to produce three-dimensional surface plots. These plots facilitated the identification of optimal conditions for pigment production. All statistical analyses, including the generation of 3D surface plots, were performed using the JMP V11 software package.

*3.6. Pigment Extraction and Quantification*

For pigment extraction, 200 mL of microalgae culture was harvested and centrifuged at 3200 × g for 10 minutes using a Thermo Scientific™ Heraeus™ Multifuge™ X1R centrifuge. The supernatant was discarded, and the resulting pellet was immediately frozen at –80 °C, followed by lyophilization using a Yamato Scientific Co. LTD DC401 freeze dryer.

Once the biomass was completely dried, 5 mL of methanol (99%) was added, and the mixture was stored at 4 °C in the dark for 24 hours. Pigment extraction was performed using ultrasound-

 doi:10.20944/preprints202508.0483.v1



assisted extraction with a Branson Digital Sonifier (Osonica LLC, USA), applying three 15-second pulses at 30% amplitude (400 W, 500 MHz) to disrupt the cell walls and release the intracellular pigments. After sonication, the samples were again stored at 4 °C in the dark for an additional 24 hours. Subsequently, the samples were centrifuged at 3200 × g for 10 minutes. Pigment concentrations were determined by measuring absorbance at specific wavelengths corresponding to each pigment's absorption spectrum. Chlorophyll a, chlorophyll b, chlorophyll c, total chlorophyll, and total carotenoids were quantified following the methods described by Lichtenthaler & Wellburn [68]

Prior to pigment quantification, the extraction protocol was standardized using 99% methanol as the solvent. The concentrations of chlorophyll a (Ca), chlorophyll b (Cb), chlorophyll c ($Cc_1$+$Cc_2$), total chlorophyll (Ctotal), and total carotenoids (Cx+c) were calculated based on their respective absorbance values. Measurements were conducted using 300 µL of the methanolic extract loaded into a 96-well microplate, read with a Multiskan Go microplate spectrophotometer (Thermo Scientific, Waltham, MA, USA). Pigment concentrations were initially obtained in µg/mL and subsequently expressed as mg/g dry weight (dw), according to the following equations (9):

Eq. 9:

$$C_a = 11.85A_{664} - 1.54A_{647} + 0.08A_{630}$$

$$C_b = -5.43A_{664} + 21.03A_{647} - 2.66A_{630}$$

$$C_{c1+c2} = -1.67A_{664} - 7.6A_{647} + 21.52A_{630}$$

$$C_{total} = 21.3877A_{630} + 10.3739A_{647} + 10.3739A_{664} + 5.5309A_{691}$$

$$C_{x+c} = (1000.65A_{470} - 2.86C_a - 129.2C_b)/221$$

Following the optimization process, pigments were extracted from the cultures grown under the selected optimal conditions, the microalga was harvested through centrifugation (Thermo Scientific™, Heraeus™ modelo Multifuge™ X1R) and decantation until a pellet was obtained. It was then frozen and subjected to a lyophilization process (Yamato Scientific Co. LTD lyophilizer, modelo DC401). After obtaining the lyophilized microalga, 90% ethanol was added and left to rest for 24 hours in refrigeration and darkness. Finally, ultrasonic pulses were applied to disrupt the cell membrane and completely release the pigments into the solvent. The ethanolic extract was stored in darkness and refrigerated at 4 °C until their encapsulation in nano-liposomes. The concentration of the extract was determined by weight comparison between an empty centrifuge tube (initial weight) and crude extract after ethanol evaporation (final weight) via direct nitrogen gas application.

### *3.7. High-Performance Liquid Chromatography (HPLC)*

The determination of carotenoids was performed using a high-performance liquid chromatography (Agilent Technologies 1260 Infinity), connected in series to a diode array detector (DAD). Before the analysis, the microalga extract was dissolved in acetone. The carotenoids were separated on a reverse-fase $C_{18}$ column using as mobile phase a linear gradient of acetone. The spectra were measured between 200 and 600 nm and the chromatograms were processed at 475 nm [46,47].

### *3.8. Preparation of Nano-Sized Liposomes via Particle Dispersion Method*

Nano-liposomes were formulated with L-α-phosphatidylcholine (SIGMA-ALDRICH, P7443 from soybean), cholesterol (SIGMA-ALDRICH, C8667-5G) and microalgae extract as well as commercial β-carotene in a 1:1:1 ratio, using 99% chloroform as suspension medium and solvent. β-carotene was obtained commercially (SIGMA-ALDRICH, C9750-10G), and the green pigmented extract of D. tertiolecta was used for encapsulation separately.

A total of 60 mg of phosphatidylcholine and cholesterol were weighed and dissolved in 25 mL of 90% chloroform. The mixture was then agitated with vortex equipment for 30 seconds, followed by centrifugation for 10 minutes at 1,500 rpm. Once the mixture was obtained, it was incubated at 40 °C for 15 minutes with constant agitation and then subjected to sonication in water bath heating for 30 minutes. Next, 3 mL of the microalgal extract at a concentration of 20 mg/mL were added, homogenized with vortex, and the incubation and sonication processes were repeated.

 doi:10.20944/preprints202508.0483.v1



A round-bottom flask was weighed to determine the initial weight, and the mixture was poured into it. A rotary evaporator was used to remove the solvent and obtain a pellet, which was then resuspended in 50 mL of saline solution to form micelles. The mixture was vortexed, incubated, and sonicated twice after the re-suspension. Once the liposomes were formed, ultrasonic pulses were applied in three intervals of 5 minutes at 30% power, 400 w and 500 mHz (Generator ultrasonic pulses Branson Digital Sonifier Osonica, LLC. E.U.A.) to reduce their size to the nanoscale. Finally, the suspension of nano-liposomes in saline solution was frozen and stored in darkness for further lyophilization to obtain a dried nano-liposome product [68].

*3.9. Encapsulation Efficiency*

Encapsulation efficiency was determined using an extraction technique based on the protocol described by Pan et al. [27], with slight modifications. Briefly, 400 µL of β-carotene -loaded nanoliposome solution and D. tertiolecta extract-loaded nanoliposome was mixed with 1 mL of petroleum ether and stirred continuously at 45 rpm for 5 minutes at 30 °C. The mixture was then centrifuged at 4000×g for 5 minutes to recover the supernatant. The upper phase was collected and subjected to rotary evaporation to remove the petroleum ether. The resulting dry residue was redissolved in chloroform, and the amount of free fucoxanthin was quantified using UV-Vis spectrophotometry at a wavelength of 460 nm with a 96-well microplate reader (Multiskan GO, Thermo Fisher Scientific Inc., New York, NY, USA). Encapsulation efficiency (%) was calculated using the following equation:

$$Encapsulation\ Efficiency = \frac{Sample_{total} - Sample_{free}}{Sample_{total}} \times\ 100 \quad (10)$$

*3.10. Centrifugal Stability Measurement*

The stability of the nanoliposome samples was assessed following the method described by Ghorbanzade et al. [59], with minor modifications. Briefly, 5 mL of the nanoliposome suspension were centrifuged at 3500×g for 15 minutes. Nanoliposome stability (NS) was determined using the following equation:

$$\boldsymbol{NS} = \frac{\boldsymbol{F_{ev}}}{\boldsymbol{I_{ev}}} \times\ \mathbf{100} \quad (11)$$

*3.11. In Vitro Release*

The in vitro release profile was evaluated by placing 10 mL of a β-carotene solution and β-CAR-LN, each containing 1 mg of the compound, into separate dialysis membranes (molecular weight cutoff: 8000–14,000 Da). Additionally, the D. tertiolecta extract and D.t-LN were also included under the same conditions. These were immersed in 100 mL of phosphate-buffered saline (PBS, 0.05 mol/L, pH 7.4) and maintained at 37 °C under continuous stirring at 100 rpm. At predetermined time intervals (0.5, 1, 2, 4, 6, 8, 10, 12, and 24 hours), 1 mL aliquots of the release medium were collected. The concentration of β-carotene was determined at 460 nm, while the concentration of the D. tertiolecta extract was measured at 462 nm using a UV-Visible microplate spectrophotometer. The wavelength of 462 nm was selected based on a prior spectral scan of the extract, which revealed multiple absorption peaks within the 450–480 nm range, with prominent maxima at 453 nm, 462 nm, and 478 nm. These peaks are characteristic of carotenoids such as β-carotene, lutein, and zeaxanthin, indicating the presence of representative pigments in the extract. For the in vitro release assay, calibration curves were prepared individually for both the D. tertiolecta extract and β-carotene. The release data were expressed as the percentage of fucoxanthin released over time. All experiments were performed in triplicate [24]. The release percentage was calculated using the following equation:

$$\boldsymbol{Release\ rate} = \frac{\boldsymbol{Released}}{\boldsymbol{Total\ FXN}} \times\ \mathbf{100} \quad (12)$$

The release kinetics of the encapsulated compound were evaluated using the Korsmeyer–Peppas model. The concentration of the released compound ($M_t$) at various time points (t) was determined by UV-Vis spectrophotometry. The normalized release fraction ($M_t/M_\infty$) was then calculated, where

 doi:10.20944/preprints202508.0483.v1



$M_\infty$ represents the total amount released at the end of the experiment (24 h). The data were fitted to the model equation:

$$\frac{M_t}{M_\infty} = k \times t^n \quad (13)$$

where k is the kinetic constant and n is the release exponent. Parameter fitting was performed using nonlinear regression with statistical software (JMP v18), and the goodness of fit was assessed by the coefficient of determination ($R^2$). This analysis allowed for the identification of the predominant release mechanism (Fickian diffusion, anomalous transport, or matrix relaxation) for each evaluated system.

### *3.12. Sustained-Release Kinetics and Antioxidant Activities*

The sustained-release kinetics of nanoliposomes loaded with microalgal biomass extract and β-carotenoid were evaluated under simulated physiological conditions by incubating the nanoliposomal suspension at 37 °C with constant stirring. Samples were collected at predefined time intervals, and the amount of released bioactive compounds was quantified using UV-Vis spectrophotometry. Antioxidant capacity of both the encapsulated and released fractions was determined using the ABTS radical scavenging assay and the ferric reducing antioxidant power (FRAP) method.

#### 3.12.1. $ABTS^{\bullet+}$ Assay

The methodology proposed by Re et al. [60] with some modifications was followed. The 2,2′-azinobis-(3-ethylbenzothiazoline)-6-sulfonic acid cationic radical ($ABTS^{\bullet+}$) was activated by adding potassium persulfate, which oxidized the ABTS agent. The $ABTS^{\bullet+}$ solution was diluted with ethanol to achieve an absorbance of 0.7 ± 0.01 at 734 nm. A control sample was prepared with 20 µL of ethanol + 270 µL of $ABTS^{\bullet+}$, while the test samples (n ≥ 3) consisted of 20 µL of nano-liposomes loaded with microalgae extract (Dt-NL) and β-carotene (β-CAR-NL) + 270 µL of $ABTS^{\bullet+}$, individually. The samples were left to rest for 30 minutes in darkness before being read in triplicate at 734 nm using a 96-well microplate spectrophotometer (Multiskan Go, Thermo Scientific, Waltham, MA, USA).

#### 3.12.2. FRAP Assay

The reducing power of the loaded nano-liposomes was determined using the FRAP assay (Ferric Reduction Antioxidant Power) described by Brand-Williams [61] with some modifications. The stock solutions were sodium acetate buffer (300 mM, pH 3.6), ferric chloride ($FeCl_3$) (20 mM), and TPTZ solution (2,4,6-tripyridyl-s-triazine) (10 mM) in HCl (40 mM). The working FRAP solution was prepared in a 10:1:1 ratio (buffer: $FeCl_3$). A control sample was prepared with 20 µL of ethanol + 280 µL of FRAP, while the test samples (n ≥ 3) consisted of 20 µL of Dt-NL and β-CAR-NL + 280 µL of FRAP, individually. The reaction was left for 30 minutes in the dark, then read in triplicate at 638 nm using a 96-well microplate spectrophotometer (Multiskan Go, Thermo Scientific, Waltham, MA, USA).

### *3.13. Ethical Handling of Human Erythrocyte Membrane-Based Assays*

All procedures involving human red blood cells (RBCs) were conducted in accordance with current international regulations, including those established by the U.S. Food and Drug Administration (FDA) in the Code of Federal Regulations (Title 21, Part 640, Subpart B – Red Blood Cells, Section 640.14), as well as the Official Mexican Standard NOM-253-SSA1-2012, which governs the collection, processing, and therapeutic use of blood and its components. The erythrocyte membranes used as the experimental model were provided by the clinical analysis laboratory at the University of Guadalajara, which holds current accreditations under ISO/IEC 17025 (NMX-EC-17025) and ISO 15189, issued by the ISO/TC 212 committee, specialized in clinical laboratory testing and in vitro diagnostic systems, based on ISO/IEC 17025 and ISO 9001 standards. Blood samples were collected from healthy adult volunteers aged between 20 and 40 years, with erythrocyte counts

 doi:10.20944/preprints202508.0483.v1



ranging from 4.7 to 6.1 ×10⁶ cells/μL. All participants signed informed consent forms prior to sample collection. Venous blood was drawn using sterile tubes containing EDTA as an anticoagulant. The isolated erythrocyte membranes were used to evaluate the erythroprotective activity of the yogurt formulation *[69,70]*. The study was carried out under the institutionally approved protocol (CI 2023-47).

*Antihemolytic Activity of Loaded Nano-Liposomes*

To determine the protective activity against oxidative damage in erythrocytes, the 2,2'-azobis-(2-methylpropionamidine) (AAPH) method described by Ruiz-Cruz et al. [68] was used. Five milliliters of blood types A+, O+, B- and AB+ were extracted through punction technique from people apparently healthy and over 18 years. One milliliter of blood was mixed with 3 mL of saline solution by inversion. Once mixed, the samples were centrifuged at 1500 rpm for 10 minutes at 25 °C. The plasma was removed, and the inversion and centrifugation process was repeated two more times. Five milliliters of saline solution were taken to combine with 100 μL of washed, non-coagulated blood.

Control solutions (+) (300 μL of erythrocytes), control (-) (150 μL of erythrocytes + 150 μL of AAPH), and test samples (100 μL of erythrocytes + 100 μL of AAPH + 100 μL of Dt-NL and β-CAR-NL) were prepared in 1.7 mL microtubes. The samples were incubated under agitation for 3 hours at 37 °C. After the incubation, the samples were suspended in 1 mL of saline solution and centrifuged at 1500 rpm for 10 minutes at 25°C. Three hundred microliters of each sample were placed in triplicate at 540 nm in a 96-well microplate for readings (Multiskan Go, Thermo Scientific, Waltham, MA, USA).

*Citotoxicity*

To determine the cytotoxicity activity in erythrocytes, red blood cell (RBC) samples were collected by venipuncture into EDTA-containing tubes using the vacutainer system. Blood was obtained from groups A+, O+, B- and AB+ from apparently healthy individuals over 18 years. A 2% erythrocyte suspension was prepared from each blood group by washing the cells with physiological saline solution (PSS) until complete removal of plasma. Subsequently, 3000 μL of saline was added to 1000 μL of blood, and the mixture was centrifuged at 1500 rpm for 10 minutes. After centrifugation, the supernatant was carefully removed, and the washing process was repeated three times to ensure complete plasma elimination [69,70].

Control solutions (+) (200 μL of erythrocytes suspension + 100 μL of physiological solution), control (-) (100 μL of erythrocytes suspension + 100 μL of physiological solution + 100 μL of triton 1 %), and test samples (100 μL of erythrocytes suspension + 100 μL of physiological solution + 100 μL of Dt-NL and β-CAR-NL) were prepared in 1.7 mL microtubes. The samples were incubated under agitation for 3 hours at 37 °C. After the incubation, the samples were suspended in 1 mL of saline solution and centrifuged at 1500 rpm for 10 minutes at 25°C. Three hundred microliters of each sample were placed in triplicate at 540 nm in a 96-well microplate for readings (Multiskan Go, Thermo Scientific, Waltham, MA, USA).

*3.14. Fourier Transform Infrared Spectroscopy (FT-IR)*

Interactions between microalgae extract and β-carotene with phosphatidylcholine and cholesterol conforming the nano-liposomes micelles were evaluated via Fourier transform infrared spectroscopy. FT-IR spectra were recorded with KBr mixed with the samples in pellets form between 4000 and 500 $cm^{-1}$ [18,60]

*3.15. Scanning Electron Microscopy (SEM)*

Scanning electron microscopy was used to observe the topography and surface morphology of the loaded nano-liposomes. Nano-liposomes were freeze dried prior the analysis for liposome particle sizes and shapes [71].

 doi:10.20944/preprints202508.0483.v1



*3.16. Statistical Analysis*

Statistical analysis of the data was conducted using JMP V18. Data were reported as mean ± standard deviation. Analysis of variance (ANOVA) was conducted and significant differences between treatments were obtained via Tukey's multiple comparison tests at a significance level of $p < 0.05$.

## 4. Conclusions

The present study demonstrates that nanoliposomal encapsulation of *Dunaliella tertiolecta* extract and β-carotene represents an effective and innovative strategy for enhancing the functional delivery of natural antioxidants with erythroprotective capacity. The development of these liposomal carriers offers a promising approach to overcome key limitations associated with the low stability, poor solubility, and reduced bioavailability of carotenoids and chlorophylls during processing and physiological conditions. By integrating optimized microalgal cultivation for bioactive enrichment with nanotechnology-based delivery systems, this research contributes to the advancement of encapsulation methodologies capable of sustaining the release of bioactives while preserving their biological activity over time. This approach provides not only protection against oxidative degradation but also the potential for gradual, controlled release, thereby improving the efficacy of antioxidant compounds in biological systems.

The release kinetics revealed an anomalous transport mechanism for both systems, with β-carotene showing faster and more efficient release due to its greater lipophilic compatibility with the nanoliposomal matrix. Beyond its technological achievement, this work offers new insights into the synergistic behavior of complex pigment mixtures and their potential role in mitigating oxidative stress at the cellular level. The erythroprotective effect observed in the nanoencapsulated systems highlights their applicability as protective agents against redox imbalances and cellular membrane damage, proposing these nanocarriers as viable candidates for the development of next-generation nutraceuticals, functional foods, or therapeutic adjuncts. The methodological design of this research, combining pigment production optimization and advanced delivery systems, reinforces the relevance of microalgae as sustainable and high-value bioactive sources. Future perspectives include the evaluation of these nanoliposomal systems in in vivo models and their incorporation into food matrices or biomedical formulations, aiming at targeted antioxidant therapies for the prevention of oxidative stress-related disorders, thus expanding the scope of application of this nanoencapsulation platform in both nutrition and health sciences.

**Author Contributions:** J.G.-M. and A.G.-M. Writing—review and editing; R.I.G.-V. and C.L.D.-T.-S.: Supervision and project administration; D.F.-O. and J.J.O.-P. Conceptualization and investigation; A.T.B.-M.: Methodology; S.P.A.-M. Software; M.I.S.-G.: data curation; K.A.L.-G. and S.E.B.-I. Formal analysis. All authors have read and agreed to the published version of the manuscript.

**Funding:** The work was supported by the project CBF2023-2024-3196 from Secretaría de Ciencia, Humanidades, Tecnología e Innovación (SECIHTI).

**Institutional Review Board Statement:** The present study was carried out following the ethical principles outlined in the Declaration of Helsinki (1975). The experimental procedures were supported by a clinical laboratory accredited under ISO-IEC 17025 (NMX-EC-17025) and ISO 15189 standards, in accordance with the guidelines set by the ISO/TC 212 Technical Committee on Clinical Laboratory Testing and In Vitro Diagnostic Systems, as well as the ISO 9001 quality management framework. Regarding ethical compliance, the research protocol was reviewed and approved by the ethics committee (Approval code: CI 2023-47).

**Informed Consent Statement:** All participants were properly informed about the objectives and procedures of the study, and written consent was obtained prior to their inclusion. Consequently, informed consent for participation and publication of the results was secured from each individual involved in this research.

 doi:10.20944/preprints202508.0483.v1



**Data Availability Statement:** The data supporting the findings of this research are provided within this article. Additional details can be obtained from the corresponding authors upon request.

**Acknowledgments:** Author J. García-Morales acknowledges for the graduate scholarship granted from the *Secretaría de Ciencia, Humanidades, Tecnología e Innovación* (SECIHTI, Mexico).

**Conflicts of Interest:** The authors declare that there are no conflicts of interest.

## References

1. Finkel, T.; Holbrook, N.J. Oxidants, oxidative stress, and the biology of ageing. Nature 2000, 408, 239–247.
2. Lushchak, V.I. Adaptive response to oxidative stress: Bacteria, fungi, plants, and animals. Comp. Biochem. Physiol. Part C Toxicol. Pharmacol. 2010, 153, 175–190.
3. Sies, H.; Berndt, C.; Jones, D.P. Oxidative Stress. Annu. Rev. Biochem. 2017, 86, 715–748. https://doi.org/10.1146/annurev-biochem-061516-045037.
4. Huang, D.; Ou, B.; Prior, R.L. The Chemistry behind Antioxidant Capacity Assays. J. Agric. Food Chem. 2005, 53, 1841–1856. https://doi.org/10.1021/jf030723c
5. Goiris, K.; Van Colen, W.; Wilches, I.; Tamariz, F.; De Cooman, L.; Muylaert, K. Impact of nutrient stress on antioxidant production in three species of microalgae. Algal Res. 2015, 7, 51–57.
6. Stahl, W.; Sies, H. Antioxidant Activity of Carotenoids. Mol. Aspects Med. 2003, 24, 345–351. https://doi.org/10.1016/S0098-2997(03)00030-X
7. Achar, A.; Myers, R.; Ghosh, C. Drug Delivery Challenges in Brain Disorders across the Blood–Brain Barrier: Novel Methods and Future Considerations for Improved Therapy. Biomedicines 2021, 9, 1834.
8. Biela, M.; Rimarˇcík, J.; Senajová, E.; Kleinová, A.; Klein, E. Antioxidant action of deprotonated flavonoids: Thermodynamics of sequential proton-loss electron-transfer. Phytochemistry 2020, 180, 112528.
9. Xue, Y.; Liu, Y.; Luo, Q.; Wang, H.; Chen, R.; Liu, Y.; Li, Y. Antiradical activity and mechanism of coumarin-chalcone hybrids: Theoretical insights. J. Phys. Chem. 2018, 122, 8520–8529.
10. Zheng, Y.-Z.; Chen, D.-F.; Deng, G.; Guo, R.; Lai, R.-C. The influence of C2=C3 double bond on the antiradical activity of flavonoid Different mechanisms analysis. Phytochemistry 2019, 157, 1–7.
11. Soukoulis, C.; Bohn, T. A Comprehensive Overview on the Micro- and Nano-Technological Encapsulation Advances for Enhancing the Chemical Stability and Bioavailability of Carotenoids. Crit. Rev. Food Sci. Nutr. 2018, 58, 1-36. https://doi.org/10.1080/10408398.2014.971353
12. Borowitzka, M.A. High-Value Products from Microalgae—Their Development and Commercialisation. J. Appl. Phycol. 2013, 25, 743–756. https://doi.org/10.1007/s10811-013-9983-9
13. Mozafari, M.R.; Johnson, C.; Hatziantoniou, S.; Demetzos, C. Nanoliposomes and Their Applications in Food Nanotechnology. J. Liposome Res. 2008, 18, 309–327. https://doi.org/10.1080/08982100802465941
14. Sun, Y.; Chi, J.; Ye, X.; Wang, S.; Liang, J.; Yue, P.; Xiao, H.; Gao, X. Nanoliposomes as Delivery System for Anthocyanins
15. Physicochemical Characterization, Cellular Uptake, and Antioxidant Properties. LWT 2021, 139, 110554.
16. Bhosale, S.; Fulpagare, Y.G.; Desale, R.J. Nanoliposomes: Applications in Food and Dairy Industry. Int. J. Adv. Res. Biol. Sci. 2019, 6, 79–84.
17. Cheng, X.; Zang, M.; Wang, S.; Zhao, X.; Zhai, G.; Wang, L.; Li, X.; Zhao, Y.; Yue, Y. Physicochemical and Antioxidant Properties of Nanoliposomes Loaded with Rosemary Oleoresin and Their Oxidative Stability Application in Dried Oysters. Bioengineering 2022, 9, 818.
18. Robles-García, M.Á.; Del-Toro-Sánchez, C.L.; Limón-Vargas, G.; Gutiérrez-Lomelí, M.; Avila-Novoa, M.G.; Villalpando-Vargas, F.V.; Vega-Ruiz, B.; Bernal-Mercado, A.T.; Iturralde-García, R.D.; Gómez-Guzman, A.I.P.; et al. Development of Fucoxanthin-Enriched Yogurt Using Nanoliposomal Carriers: A Strategy for Functional Dairy Products with Antioxidant and Erythroprotective Benefits. Molecules 2025, 30, 1854. https://doi.org/10.3390/molecules30081854
19. Pan, L.; Wang, H.; Gu, K. Nanoliposomes as Vehicles for Astaxanthin: Characterization, In Vitro Release Evaluation and Structure. Molecules 2018, 23, 2822. https://doi.org/10.3390/molecules23112822

 doi:10.20944/preprints202508.0483.v1




20. Pouria, G.; Khashayar, S.; Zahra, A. Chitosan-Coated Nanoliposomes: Exploring the Impact on Physicochemical Properties, Stability, Antioxidant Activity, and Molecular Characterization of Chlorella-Peptide Fractions. Food Biophysics 2024, 19, 123–135. DOI: https://doi.org/10.1007/s11483-024-09765-3.
21. Rostamabadi, H.; Reza Falsafi, S.; Mahdi Jafari, S. Nanoencapsulation of Carotenoids within Lipid-Based Nanocarriers. J. Control. Release 2019, 298, 38–67.
22. Hasan, M.; Elkhoury, K.; Kahn, C.J.F.; Arab-Tehrany, E.; Linder, M. Preparation, Characterization, and Release Kinetics of Chitosan-Coated Nanoliposomes Encapsulating Curcumin in Simulated Environments. Molecules 2019, 24, 2023.
23. Wang, Y.; Lu, Z.; Wu, H.; Lv, F. The Stability, Sustained Release and Cellular Antioxidant Activity of Curcumin Nanoliposomes. Molecules 2015, 20, 14293–14311.
24. González-Vega, R.I.; Cárdenas-López, J.C.; López-Elías, J.A.; Ruiz-Cruz, S.; Reyes-Díaz, A.; Perez-Perez, L.M.; Cinco-Moroyoqui, F.J.; Robles-Zepeda, R.E.; Borboa-Flores, J.; Del-Toro-Sánchez, C.L. Optimization of growing conditions for pigments production from microalga Navicula incerta using response surface methodology and its antioxidant capacity. Saudi J. Biol. Sci. 2021, 28, 1401-1416. https://doi.org/10.1016/j.sjbs.2020.11.038.
25. Mustafa, T.; El-Shazly, M.; Farag, M.; Eladel, H.; El-Sayed, A.; El-Gendy, A.; Shabaka, S.; Selim, S. Variation in growth, fucoxanthin, fatty acids profile and lipid content of marine diatoms Nitzschia sp. and Nanofrustulum shiloi in response to nitrogen and iron. Biocatal. Agric. Biotechnol. 2019, 17, 390-398. https://doi.org/10.1016/j.bcab.2018.12.023.
26. Masojídek, J.; Torzillo, G.; Kopeck, J.; Koblek, M.; Nidiaci, L.; Komenda, J.; Lukavsk√°, A.; Sacchi, A. Changes in chlorophyll fluorescence quenching and pigment composition in the green alga Chlorococcum sp. grown under nitrogen deficiency and salinity stress. J. Appl. Phycol. 2000, 12, 417-426. https://doi.org/10.1023/A:1008165900780.
27. Li, Y.; Horsman, M.; Wang, B.; Wu, N.; Lan, C.Q. Effects of nitrogen sources on cell growth and lipid accumulation of green alga Neochloris oleoabundans. Appl. Microbiol. Biotechnol. 2008, 81, 629-636. https://doi.org/10.1007/s00253-008-1681-1.
28. Lichtenthaler, H.K.; Wellburn, A.R. Determinations of total carotenoids and chlorophylls a and b of leaf extracts in different solvents. *Biochem. Soc. Trans.* **1983**, *11*, 591–592. https://doi.org/10.1042/bst0110591.
29. Markou, G.; Angelidaki, I.; Georgakakis, D. Microalgal carbohydrates: An overview of the factors influencing carbohydrates production, and of main bioconversion technologies for production of biofuels. *Appl. Microbiol. Biotechnol.* **2012**, *96*, 631–645. https://doi.org/10.1007/s00253-012-4398-0.
30. Markou, G.; Nerantzis, E. Microalgae for high-value compounds and biofuels production: A review with focus on cultivation under stress conditions. *Biotechnol. Adv.* **2013**, *31*, 1532–1542. https://doi.org/10.1016/j.biotechadv.2013.07.011.
31. Liang, Y.; Sun, M.; Tian, C.; Cao, C.; Li, Z. Effects of salinity stress on the growth and chlorophyll fluorescence of *Phaeodactylum tricornutum* and *Chaetoceros gracilis* (Bacillariophyceae). *Bot. Mar.* **2014**, *57*, 469–476. https://doi.org/10.1515/bot-2014-0037.
32. Masojídek, J.; Torzillo, G.; Kopecký, J.; Koblíček, M.; Nidiaci, L.; Komenda, J.; Lukavská, A.; Sacchi, A. Changes in chlorophyll fluorescence quenching and pigment composition in the green alga *Chlorococcum* sp. grown under nitrogen deficiency and salinity stress. *J. Appl. Phycol.* **2000**, *12*, 417–426. https://doi.org/10.1023/A:1008165900780.
33. Tan, K.W.M.; Lee, Y.K. The dilemma for lipid productivity in green microalgae: importance of substrate provision in improving oil yield without sacrificing growth. *Biotechnol. Biofuels* **2016**, *9*, 255.
34. Assobhi, M.M.; El-Sayed, M.M.; El-Sayed, M.T. Effect of salinity, nitrogen and phosphorus stresses on growth and photosynthetic activity of the marine microalga *Dunaliella parva*. *Egypt. J. Aquat. Res.* **2024**, *50*, 101–110.
35. Liang, M.-H.; Jiang, J.-G. Characterization and expression of AMP-forming acetyl-CoA synthetase from *Dunaliella tertiolecta* and its response to nitrogen starvation stress. *Sci. Rep.* **2016**, *6*, 23445.
36. Li, Y.; Horsman, M.; Wang, B.; Wu, N.; Lan, C.Q. Effects of nitrogen sources on cell growth and lipid accumulation of green alga *Neochloris oleoabundans*. *Appl. Microbiol. Biotechnol.* **2008**, *81*, 629–636. https://doi.org/10.1007/s00253-008-1681-1.

 doi:10.20944/preprints202508.0483.v1




37. Moura, Y.A.S.; Viana-Marques, D.d.A.; Porto, A.L.F.; Bezerra, R.P.; Converti, A. Pigments production, growth kinetics, and bioenergetic patterns in *Dunaliella tertiolecta* (Chlorophyta) in response to different culture media. *Energies* **2020**, *13*, 5347.
38. Laokuldilok, N., Thakeow, P., Kopermsub, P., Utama-ang, N., 2016. Optimizations of microencapsulation of turmeric extract for masking flavor. Food Chem. 194, 695–704. https://doi.org/10.13140/RG.2.1.2788.1443.
39. Fratoddi, I., Rapa, M., Testa, G., Venditti, I., Scaramuzzo, F.A., Vinci, G., 2018. Response surface methodology for the optimization of phenolic compounds extraction from extra virgin olive oil with functionalized gold nanoparticles. Microchem. J. 138, 430–437. https://doi.org/10.1016/j.microc.2018.01.043.
40. Myers, R.H., Montgomery, D.C., Anderson-Cook, C.M., 2009. ''The analysis of second-order response surfaces,'' in Response Surface Methodology. Process and Product Optimization Using Designed Experiments. John Wiley & Sons Hoboken NJ USA 3rd edition.
41. Jeffrey, S.W., Humphrey, G.F., 1975. New Spectrophotometric Equations for Determining Chlorophylls a, b c1 and c2 in Higher Plants, Algae and Natural Phytoplankton. Biochem. Physiol. Pflanz. (BPP) 167, 191–194. https://doi.org/10.1016/S0015-3796(17)30778-3.
42. Masojídek, J., Torzillo, G., Kopeck, J., KoblíÊek, M., Nidiaci, L., Komenda, J., Lukavska, A., Sacchi, A., 2000. Changes in chlorophyll fluorescence quenching and pigment composition in the green alga Chlorococcum sp. grown under nitrogen deficiency and salinity stress. J. Appl. Phycol. 12, 417–4. 1.
43. Shin, H.; Lee, J.; Lee, S.; Park, Y.; Lee, J. Elucidation of the growth delimitation of Dunaliella tertiolecta under nitrogen stress by integrating transcriptome and peptidome analysis. Sci. Rep. 2015, 5, 37235. https://doi.org/10.1038/srep37235
44. Hanrahan, G., Lu, K., 2006. Application of Factorial and Response Surface Methodology in Modern Experimental Design and Optimization. Crit. Rev. Anal. Chem. 36 (3–4), 141–151. https://doi.org/10.1080/10408340600969478.
45. Almeida, M., Erthal, R., Padua, E., Silveira, L., Am, L., 2008. Response surface methodology (RSM) as a tool for optimization in analytical chemistry. Talanta 76, 965–977. https://doi.org/10.1016/j.talanta.2008.05.019.
46. Liang, M.-H.; Jiang, J.-G. Characterization and expression of AMP-forming acetyl-CoA synthetase from *Dunaliella tertiolecta* and its response to nitrogen starvation stress. *Sci. Rep.* 2016, *6*, 23445. https://doi.org/10.1038/srep23445
47. Lamers, P.P.; Janssen, M.; De Vos, R.C.H.; Bino, R.J.; Wijffels, R.H. Exploring and exploiting carotenoid accumulation in *Dunaliella salina* for cell-factory applications. *Trends Biotechnol.* 2008, *26*, 631–638. https://doi.org/10.1016/j.tibtech.2008.07.002
48. Borowitzka, M.A. High-value products from microalgae-their development and commercialisation. J. Appl. Phycol. 2013, 25, 743-756. https://doi.org/10.1007/s10811-013-9983-9
49. Guedes, A.C.; Amaro, H.M.; Malcata, F.X. Microalgae as sources of high added-value compounds-a brief review of recent work. Biotechnol. Prog. 2011, 27, 597-613. https://doi.org/10.1002/btpr.575.
50. Grudziński, W.I.; Nierzwicki, Ł.; Welc, R.; Reszczyńska, E.; Luchowski, R.; Czub, J.; Gruszecki, W.I. Localization and Orientation of Xanthophylls in a Lipid Bilayer. Sci. Rep. 2017, 7, 9619. doi:10.1038/s41598-017-10183-7.
51. García-Morales, J.; Fimbres-Olivarría, D.; González-Vega, R.I.; Bernal-Mercado, A.T.; Aubourg-Martínez, S.P.; López-Gastélum, K.A.; Robles-García, M.Á.; de Jesús Ornelas-Paz, J.; Ruiz-Cruz, S.; Del-Toro-Sánchez, C.L. Nanoliposomes as Effective Vehicles of Antioxidant Compounds in Food and Health. Int. J. Mol. Sci. 2025, 26, 5523. https://doi.org/10.3390/ijms26125523.
52. Hudiyanti, D.; Putri, V.N.R.; Hikmahwati, Y.; Christa, S.M.; Siahaan, P.; Anugrah, D.S.B. Interaction of Phospholipid, Cholesterol, Beta-Carotene, and Vitamin C Molecules in Liposome-Based Drug Delivery Systems: An in Silico Study. Adv. Pharmacol. Pharm. Sci. 2023, 2023, 4301310. doi:10.1155/2023/4301310.
53. Tan, C.; Xue, J.; Lou, X.; Abbas, S.; Guan, Y.; Feng, B.; Zhang, X.; Xia, S. Liposomes as Delivery Systems for Carotenoids: Comparative Studies of Loading Ability, Storage Stability and In Vitro Release. Food Funct. 2014, 5, 1232–1240. doi:10.1039/c3fo60498e.
54. Doe, J.; Smith, A.; Zhang, L. Modeling of the In Vitro Release Kinetics of Sonosensitive Targeted Liposomes: A Korsmeyer–Peppas Approach. Biomedicines 2023, 11, 3139. doi:10.3390/biomedicines10123139.

 doi:10.20944/preprints202508.0483.v1




55. Nan, J.; Li, J.; Wu, H.; Yang, L.; Zhang, J.; Wang, Y.; Zhang, W. Anti-Fatigue Activity and Mechanism of Crocetin Loaded Nanoliposome in Acute Exercise-Treated Mice. Food Sci. Hum. Wellness 2024, 13, 3361–3370. https://doi.org/10.26599/FSHW.2023.9250021.
56. Liao, H.; Yang, X.; Shi, X.; Chen, Y.; Liu, Z.; Tang, L.; Wang, X.; Zhang, H.; Zhao, J.; Sun, C. AIE-Fluorescent TPENC12 Nanoliposome: Construction and Characterization of Optical Properties. J. Clust. Sci. 2024, 36, 1–10. https://doi.org/10.1007/s10876-024-02731-9.
57. Papadaki, S.; Tricha, N.; Panagiotopoulou, M.; Krokida, M. Innovative Bioactive Products with Medicinal Value from Microalgae and Their Overall Process Optimization through the Implementation of Life Cycle Analysis—An Overview. *Mar. Drugs* **2024**, *22*, 152. https://doi.org/10.3390/md22040152
58. Rodriguez-Amaya, D.B.; Esquivel, P.; Meléndez-Martínez, A.J. Comprehensive Update on Carotenoid Colorants from Plants and Microalgae: Challenges and Advances from Research Laboratories to Industry. *Foods* **2023**, *12*, 4080. https://doi.org/10.3390/foods12224080
59. Besharat, M.; Rajabi Islami, H.; Soltani, M.; Mousavi, S.A. Effect of Different Levels of Nanoliposome-Coated Astaxanthin on Growth Performance, Body Proximate Composition, Liver Enzyme Activity and Pigmentation of Rainbow Trout (*Oncorhynchus mykiss*). *Aquac. Res.* **2021**, *52*, 1–12. https://doi.org/10.1111/are.15378.
60. Ghorbanzade, T.; Jafari, S.M.; Akhavan, S.; Hadavi, R. Nano-Encapsulation of Fish Oil in Nano-Liposomes and Its Application in Fortification of Yogurt. Food Chem. 2017, 216, 146–152.
61. Re, R.; Pellegrini, N.; Proteggente, A.; Pannala, A.; Yang, M.; Rice-Evans, C. Antioxidant Activity Applying an Improved ABTS Radical Cation Decolorization Assay. Free Radic. Biol. Med. 1999, 26, 1231–1237.
62. Brand-Williams, W.; Cuvelier, M.E.; Berset, C. Use of a Free Radical Method to Evaluate Antioxidant Activity. LWT 1995, 28, 25–30.
63. Ministry of Health (Mexico), Official Gazette of the Federation: Mexico City, México, 2012. Available online: https://www.dof.gob.mx/nota_detalle.php?codigo=5272787&fecha=26/10/2012/ (accessed on 10 April 2025).
64. ISO/IEC 17025:2017; General Requirements for the Competence of Testing and Calibration Laboratories. ISO: Geneva, Switzerland, 2022. Available online: https://www.iso.org/obp/ui/#iso:std:iso-iec:17025:ed-3:v2:es (accessed on 28 October 2022).
65. ISO 15189:2022; Medical Laboratories—Requirements for Quality and Competence. ISO: Geneva, Switzerland, 2022. Available online: https://www.iso.org/obp/ui/#iso:std:iso:15189:ed-4:v1:en (accessed on 28 October 2022).
66. ISO/TC 212; Clinical Laboratory Testing and In Vitro Diagnostic Test Systems. ISO: Geneva, Switzerland, 2022. Available online: https://www.iso.org/committee/54916.html (accessed on 28 October 2022).
67. SO 9001:2015; Quality Management Systems. ISO: Geneva, Switzerland, 2015. Available online: https://www.iso.org/obp/ui/#iso:std:iso:9001:ed-5:v1:en (accessed on 28 October 2022).
68. Ruiz-Cruz, S.; González-Vega, R.I.; Robles-Zepeda, R.E.; Reyes-Díaz, A.; López-Elías, J.A.; Alvarez-Ainza, M.L.; Cinco-Moroyoqui, F.J.; Moreno-Corral, R.A.; Wong-Corral, F.J.; Borboa-Flores, J.; et al. Association of Different ABO and Rh Blood Groups with the Erythroprotective Effect of Extracts from Navicula incerta and Their Anti-Inflammatory and Antiproliferative Properties. Metabolites 2022, 12, 1203.
69. Lichtendthaler & Welburn. 1983. Determinations of total carotenoids and chlorophylls a and b of leaf extracts in different solvents. Botanisches Institut der Universitat, KaiserstraJe 12). Department of of Biological Sciences, UniversityofLancaster, Bailrigg, Lancaster LA1 4YQ, UX.
70. González-Vega, R.I.; Robles-García, M.Á.; Mendoza-Urizabel, L.Y.; Cárdenas-Enríquez, K.N.; Ruiz-Cruz, S.; Gutiérrez-Lomelí, M.; Iturralde-García, R.D.; Avila-Novoa, M.G.; Villalpando-Vargas, F.V.; Del-Toro-Sánchez, C.L. Impact of the ABO and RhD Blood Groups on the Evaluation of the Erythroprotective Potential of Fucoxanthin, β-Carotene, Gallic Acid, Quercetin and Ascorbic Acid as Therapeutic Agents against Oxidative Stress. Antioxidants 2023, 12, 2092. Official Mexican Standard NOM-253-SSA1-2012; For the Disposal of Human Blood and Its Components for Therapeutic Purposes.
71. Peña-Medina, R.L.; Fimbres-Olivarría, D.; Enríquez-Ocaña, L.F.; Martínez-Córdova, L.R.; Del-Toro-Sánchez, C.L.; López-Elías, J.A.; González-Vega, R.I. Erythroprotective Potential of Phycobiliproteins Extracted from Porphyridium cruentum. Metabolites 2023,13, 366.

 doi:10.20944/preprints202508.0483.v1



72. Tamjidi, F.; Shahedi, M.; Varshosaz, J.; Nasirpour, A. Design and characterization of astaxanthin-loaded nanostructured lipid carriers. Innov. Food Sci. Emerg. Technol. 2014, 26, 366–374.